NASA Contractor Report 4013

Finite Volume Solution of the Compressible Boundary-Layer Equations

Bernard Loyd and Earll M. Murman

GRANT NAG1-507
OCTOBER 1986

NASA

NASA Contractor Report 4013

Finite Volume Solution of the Compressible Boundary-Layer Equations

Bernard Loyd and Earll M. Murman
Massachusetts Institute of Technology
Cambridge, Massachusetts

Prepared for
Langley Research Center
under Grant NAG1-507

National Aeronautics
and Space Administration

**Scientific and Technical
Information Branch**

1986

Acknowledgments

Our thanks go to Professors Mark Drela and Michael Giles whose suggestions and advice contributed much to this effort.

This research was supported in part by fellowships to the first author from the *Nat. Consort. for Grad. Degrees for Minorities in Engr. (GEM)* and the *National Science Foundation.* This support is gratefully acknowledged. Additional support was received through *NASA* CFD Training Grant NGT 22-009-901 and *NASA* Langley Grant NAG1-507.

Contents

List of Figures

List of Tables

Nomenclature

f	Streamfunction in transformed equations
H	1. Stagnation enthalpy, 2. Shape factor
h	1. Enthalpy, 2. Scaling factor in grid spacing
L	Length scale
P	Pressure
q	Enthalpy flux
u	Tangential velocity
v	Normal velocity
$x,\ y$	Tangential, normal coordinate
$\alpha,\ \beta$	Parameters in transformed equations
γ	Turbulence intermittency factor
δ	Boundary layer thickness
δ^*	Displacement thickness
ϵ	Eddy viscosity
η	Factor in grid spacing, $\eta = y/\theta$
θ	Momentum thickness
μ	Viscosity
ν	Kinematic viscosity
ξ	Tangential coordinate in transformed eqs.
ρ	Density
τ	Shear stress
ψ	Streamfunction

Subscripts

e	Edge quantity
$i,\ j$	Tangential, normal index

l	Laminar
k	Kinematic (constant density)
t	Turbulent
w	Wall
∞	Free stream

Chapter 1

INTRODUCTION

This report applies a finite volume approach to the two-dimensional compressible boundary layer equations. Unlike conventional finite difference methods using similarity transformations methods we introduce no equation or coordinate transformations of any kind. Instead, we discretize the integral boundary layer equations using untransformed variables. We construct a suitable computational grid and calculate an initial solution by explicitly applying similarity concepts. The resulting numerical scheme is efficient, accurate, conceptually straightforward, and very simple. Results are given for similar and non-similar flows and compared with finite difference solutions and data.

1.1 OVERVIEW

This chapter presents a background discussion and motivation of the finite volume method and a brief summary of the method. Chapter 2 presents the governing equations in integral form, non-dimensionalization, and introduction of a stream function. It is followed by descriptions of the discretization of the governing equations and of grid generation in Chapter 3. A comparison of finite volume and conventional approaches is given in Chapter 4. Chapter 5 reviews linearization of the discretized equations and solution of the resulting matrix equation. Results for similar and non-similar test cases are presented in Chapter 6, and conclusions and recomendations in Chapter 7. Details of the implementation are given in the appendices.

1.2 BACKGROUND

Numerical solution techniques for the boundary layer equations can be classified into two categories: integral methods and finite difference methods. Integral methods are based on analytic integration of the momentum equation (and, for compressible cases, the energy equation) across the boundary layer. For example, many integral methods start with the momentum integral equation for $2-D$ incompressible flow without mass transfer:

$$\frac{d\theta}{dx} + \frac{\theta}{U_e}(H+2)\frac{dU_e}{dx} = \frac{C_f}{2}\,, \tag{1.1}$$

where θ is the momentum thickness, C_f is the skin friction coefficient, and H is the ratio of displacement and momentum thicknesses. Equation 1.1 satisfies the governing equations, not at each point in the boundary layer, but in an averaged "global" sense. Since, for a given velocity distribution, there are three unknowns in that equation, two additional relations between the unknowns must be specified. Equation 1.1 is an ordinary differential equation (ODE) in x and is easily integrated numerically given suitable initial conditions. Accuracy of the solution depends on the validity of relations chosen.

Finite difference methods model some form of the governing partial differential equations (PDE's) by difference approximations on a finite grid. Because the discrete approximations reduce to the governing equations at each grid point as the grid spacing goes to zero, calculations can be performed to any degree of accuracy. With given initial and boundary conditions, no further relations or *a priori* knowledge is required for laminar flows. Since initial conditions usually are not available, the usual recourse is to transform the PDE's to so-called similarity form. A typical approach for incompressible flow is to use the Falkner-Skan variables

$$\xi = \frac{x}{L} \qquad\qquad \eta = \frac{y\sqrt{Re}}{Lg(x)} \tag{1.2}$$

to give a third order PDE:

$$f_{\eta\eta\eta} + \alpha f f_{\eta\eta} + \beta(1 - f_\eta^2) = g^2\frac{U_e}{U_\infty}\left[f_\eta\frac{\partial f_\eta}{\partial \xi} - f_{\eta\eta}\frac{\partial f}{\partial \xi}\right]\,. \tag{1.3}$$

ξ and η are the non-dimensionalized tangential and transformed normal coordinates, respectively. f is the transformed stream function, $g(x)$ is a scale factor, and α and β are functions of the pressure gradient and g.

For similar flow the right hand side of eqn. 1.3 is zero, giving an ordinary differential equation (ODE) in the cross-stream direction that is easily solved numerically. Similarity form is valid for wedge type flows only, but is widely used for generating initial conditions for non-similar flow calculations.

The primary advantage of integral methods is their simplicity and computational efficiency. However, the additional closure relations often involve empiricism. Also, it is difficult to extend integral methods to problems with added physical processes and/or diverse boundary conditions. As a result, finite difference methods have become increasingly popular. They are extremely accurate for laminar flows and allow straightforward implementation of a variety of boundary conditions. However, the transformations to similarity variables destroy the physical transparency of the equations and are of little utility once the solution has been started. The transformations are involved, and the transformed equations are complicated to the point that individual terms are not easily identified with the physical process they represent. Furthermore, the *discrete* equations usually can not be shown to exactly conserve mass, momentum, or energy, since the governing equation is no longer in divergence form. We consider a finite *volume* approach, because that approach has proven to be accurate, yet simple, when applied to the Euler and Navier-Stokes equations.

1.2.1 Finite Volume Method

Finite volume methods approximate integral forms of conservation equations on finite cells (volumes in $3-D$). The equations are approximated by summing the fluxes of mass, momentum, and energy from neighboring cells into each cell, thereby satisfying the conservation equations over that cell. Conceptually, the approach is a blend of the integral and finite difference methods. It reduces to an integral method[1] if the number of cells is one, but is a finite difference approach in the sense that with many cells, the governing equations are satisfied locally as well as globally. The method has the accuracy and versatility of finite difference schemes, but retains the physical transparency of the governing equations.

A key part of the finite volume approach is the decoupling of the discretization of the equations from the grid generation. The equations are first discretized for an arbitrary quadrilateral cell in the physical coordinate system. The grid must be constructed to provide resolution where needed. This is in contrast to transforming the equations to a similarity type coor-

[1] If that method assumes a linear u-velocity profile.

dinate system before discretizing, whereby a rectangular grid is "built into" the transformed equations. If a different scaled coordinate system is desired, one must introduce a new transformation and discretize the resulting equations. With the finite volume approach one needs only to construct a new grid and the governing equations are always in a very simple form.

1.3 SUMMARY

We present a novel finite volume solution of the two-dimensional compressible boundary layer equations. A untransformed stream function is used to simplify the governing equations, but none of the conventional similarity type transformations or scalings are applied. Instead, we use similarity principles explicitly to calculate the initial conditions. The grid is constructed to automatically follow the boundary layer growth for both similar and non-similar flows. Finite volume discretization of the integral equations gives a set of nonlinear equations, which are linearized and solved via Newton's method. Results for several similar and non-similar test cases demonstrate good agreement with tabulated solutions, computations obtained with conventional methods, and experiment.

The method is applicable to laminar and turbulent flow. We use Sutherland's formula [Schlichting 68] and the Cebeci-Smith algebraic two layer model [Cebeci 74] to calculate the laminar and turbulent viscosities, respectively.

A variety of boundary conditions can be applied. The method makes no particular distinction between solving direct cases where the edge velocity is specified and solving inverse cases where the displacement thickness, the mass defect, or some other quantity is specified.

The novelty of our approach is the use of the integral form of the equations without transformation. Instead of incorporating similarity features into the governing equations via laborious transformations and scalings, we use similarity principles explicitly. The explicit use of similarity is much simpler than the use of conventional transformations, but gives equivalent results. The finite volume method retains the conceptual simplicity of the integral conservation equations without loosing the efficiency and advantages of conventional schemes. We recommend it both as a calculation device and as a pedagogic tool in presenting numerical boundary layer solutions.

Chapter 2

GOVERNING EQUATIONS

We present the integral form of the boundary layer equations, the equation of state, and sample boundary conditions. For convenience we nondimensionalize the variables, but we do not change the form of the conservation equations.

The discrete equations in primitive (u, v) variables allow streamwise odd-even decoupling of the v velocity profile. We eliminate these oscillations by replacing the continuity equation by a stream function, and also use the stream function to simplify convective terms in the conservation of mass and energy equations.

2.1 INTEGRAL FORM

The two-dimensional steady boundary layer equations in integral form are:

$$\oint \rho u \, dy \; - \oint \rho v \, dx \; = \; 0. \tag{2.1}$$

$$\oint u(\rho u) \, dy \; - \oint v(\rho u) \; dx = - \oint P \, dy - \oint \tau \, dx \tag{2.2}$$

$$\oint u(\rho H) \, dy - \oint v(\rho H) \, dx = - \oint q \, dx \tag{2.3}$$

where x is arclength along and y is the distance normal to a given body. Integration is taken to be counter-clockwise. u and v are tangential and

normal velocities, P is static pressure, ρ is density, and H is total enthalpy. τ and q are the shear stress and enthalpy flux:

$$\tau = (\mu_l + \mu_t)\frac{\partial u}{\partial y} \tag{2.4}$$

$$q = \left[\frac{\mu_l}{Pr_l} + \frac{\mu_t}{Pr_t}\right]\frac{\partial H}{\partial y} + \mu_l\left[1 - \frac{1}{Pr_l}\right]u\frac{\partial u}{\partial y}\,. \tag{2.5}$$

Subscripts (l) and (t) denote laminar and turbulent quantities, and Pr is the Prandtl number ($\simeq 0.7$ for laminar, and 1.0 for turbulent flows). Reynolds averaging has been done for turbulent flow.

Equations 2.1 - 2.5 are five first order relations for the variables u, v, H, τ, and q. μ, ρ, and P must be given or defined in terms of these variables. The laminar viscosity is obtained from Sutherland's law, and the Cebeci-Smith model is used to calculate the turbulent viscosity[1]. The equation of state for a perfect gas gives the density-enthalpy relation,

$$\rho = \frac{\gamma}{\gamma - 1}\frac{P}{h}\,. \tag{2.6}$$

Boundary conditions may be applied in the so-called direct or inverse mode. In either case, the normal and tangential velocities at the wall must be specified; typically, $u(x,0) = 0$, and $v(x,0) = v_w(x)$. Also, either enthalpy or enthalpy flux at the wall must be given, as well as the total enthalpy at the edge of the boundary layer. "Direct" or "inverse" refers to the specification of the remaining (fifth) boundary condition. Direct mode implies specifying the edge velocity U_e and amounts to imposing a known pressure field:

$$\int \frac{dp}{\rho} = -\frac{U_e^2}{2} \tag{2.7}$$

on the boundary layer. Alternatively, one of a number of inverse boundary conditions, for example, specified displacement thickness or wall shear, is easily applied.

Initial conditions must be specified for u, v, and H to complete the formulation. These will be discussed later.

Equations 2.1 - 2.5 are a nonlinear parabolic system. They are applicable to steady compressible, turbulent boundary layers subject to the assumptions that:

[1]See Appendices B and C, respectively

- normal velocity is small compared to the streamwise velocity,
- streamwise gradients are small compared to normal gradients, and
- boundary layer thickness δ is small compared to body curvature.

The conservation of mass and momentum equations are in standard form. The conservation of energy equation is in total enthalpy (per unit mass) form. Its simplicity and its similarity with the form of the momentum equation make the enthalpy form useful. Definition of the shear stress and enthalpy flux as separate equations gives a first order system of equations.

We solve equations 2.2 - 2.5 in their most primitive form. After non-dimensionalization, a stream function is introduced. No further equation or coordinate transformations of any kind are applied. Mass, momentum and energy are rigorously conserved in the discrete approximation.

2.2 NON-DIMENSIONALIZATION

We non-dimensionalize all variables with the freestream quantities U_∞, ρ_∞, and some characteristic length L. The primed variables, below, indicate non-dimensional values.

$$\begin{aligned}
u' &= \frac{u}{U_\infty} & v' &= \frac{v}{U_\infty} \\
P' &= \frac{P}{\rho_\infty U_\infty^2} & \psi' &= \frac{\psi}{U_\infty L} \\
H' &= \frac{H}{U_\infty^2} & q' &= \frac{q}{\rho_\infty U_\infty^3} \\
\tau' &= \frac{\tau}{\rho_\infty U_\infty^2} & \mu' &= \frac{\mu}{\rho_\infty U_\infty L} \\
x' &= \frac{x}{L} & y' &= \frac{y}{L}
\end{aligned} \tag{2.8}$$

With the present non-dimensionalization of μ the Reynolds number does not appear as an explicit parameter – it is implicitly contained in the equations. The forms of the non-dimensional governing equations, equation of state, and viscosity and turbulence models are identical to that of the dimensioned equations. For convenience we drop the primes and henceforth refer to the non-dimensional form only.

2.3 STREAM FUNCTION FORMULATION

Equations 2.1 - 2.5 can be discretized immediately. We refer to that formulation as the primitive variable formulation since the dependent variables include u and v. A disadvantage of the primitive variable formulation is its susceptibility to stream-wise odd-even decoupling of the normal velocity. The disadvantage is purely cosmetic since the cell centered results are not affected. However, the odd-even decoupling can be eliminated by introducing a stream function into the momentum and energy equations. Furthermore, introduction of the stream function into the momentum and energy equations allows reduction of the number of terms in each equation by one, yielding an increase in simplicity and computational efficiency.

2.3.1 Elimination of the continuity equation

The definition of the total derivative gives a general relation for $\psi = \psi(x, y)$:

$$d\psi = \frac{\partial \psi}{\partial y} dy + \frac{\partial \psi}{\partial x} dx \tag{2.9}$$

If now we define,

$$\frac{\partial \psi}{\partial y} = \rho u \qquad\qquad \frac{\partial \psi}{\partial x} = -\rho v \tag{2.10}$$

we recover the standard definition of the stream function

$$d\psi = \rho u dy - \rho v dx. \tag{2.11}$$

Plugging this relation into the continuity equation, it is evident that conservation of mass is identically satisfied.

Since normal gridlines are perpendicular to the surface at each streamwise station, $dx \equiv 0$ along normal gridlines; and, we can replace the continuity equation by the truncated definition of the stream function:

$$d\psi = \rho u dy_{x=const.}. \tag{2.12}$$

We apply this definition at each streamwise station, and integrate upwards at $x = const.$ to calculate ψ.

2.3.2 Simplification of momentum and energy equations

In addition to replacing the continuity equation, the stream function can simplify the convective terms in the momentum and energy equations. These terms represent the transport of x-momentum ρu and total enthalpy ρH by the u and v velocities. A simple rearrangement of the convective velocity and density terms in equations 2.2 and 2.3 gives:

$$\begin{aligned} u \cdot \rho u \, dy - v \cdot \rho u \, dx &\Rightarrow u \cdot \rho u \, dy - u \cdot \rho v \, dx \\ u \cdot \rho H \, dy - v \cdot \rho H \, dx &\Rightarrow H \cdot \rho u \, dy - H \cdot \rho v \, dx \end{aligned} \tag{2.13}$$

but, using 2.11, this is simply

$$\begin{aligned} u \cdot \rho u \, dy - u \cdot \rho v \, dx &= u d\psi \\ H \cdot \rho u \, dy - H \cdot \rho v \, dx &= H d\psi. \end{aligned} \tag{2.14}$$

2.4 GOVERNING EQUATIONS REVISITED

For convenience we collect our governing equation set; these are the equations that we discretize:

$$\begin{aligned} & d\psi = \rho u dy_{x=const.} \\ & \oint u d\psi + \oint P dy + \oint \tau dx = 0 \\ & \oint H d\psi + \oint q \, dx = 0 \\ & \tau = (\mu_l + \mu_t) \frac{\partial u}{\partial y} \\ & q = \left[\frac{\mu_l}{Pr_l} + \frac{\mu_t}{Pr_t} \right] \frac{\partial H}{\partial y} + \mu_l \left[1 - \frac{1}{Pr_l} \right] u \frac{\partial u}{\partial y} \end{aligned} \tag{2.15}$$

The continuity equation has been replaced by the definition of the stream function, and the number of terms in the conservation of mass and conservation of energy equations is reduced by one. Density is present only in the stream function.

Chapter 3

DISCRETIZATION AND GRID GENERATION

We begin by discretizing equations 2.15 in finite volume form. This form is central to the simplicity of the scheme; conservation is expressed by a summation of fluxes around each cell, and each term in the discretized equations has a clear physical interpretation.

Subsequently, we illustrate our method for generating grids for arbitrary boundary layers. Streamwise grid lines follow lines of $\eta = const.$, where $\eta = y/h$, and cross-stream grid lines are along $x = const.$ The parameter $h = h(x)$ is a scaling factor proportional to the boundary layer thickness. With this definition of the streamwise grid lines, the computational grid always extends above the boundary layer, and grid generation is easily implemented.

The final section of this chapter discusses explicit application of similarity principles to calculate an initial solution. In similar flow each variable varies as a known power of x along $\eta = const.$ At the initial station, no previous solution is available and the number of unknonws is greater then the number of equations. We start the solution by replacing the variables at $y_{i+1,j}$ by their functional equivalents at $y_{i,j}$, thus closing the system. Since the grid is constructed with streamwise faces along $\eta = const.$, calculating a starting solution is very straightforward.

3.1 FINITE VOLUME DISCRETIZATION

We adopt a box-type finite volume discretization. All variables are defined on the four nodes of a control volume (see Figure 3.1). The momentum

and energy fluxes through a given cell side are calculated by averaging the state variables at adjacent nodes. This flux calculation is second order accurate on all grids.

The governing equations discretized in this finite volume form are extremely simple. Below are the final forms of the governing equations and the corresponding discrete approximations using a box-type difference stencil. Subscripts i and j refer to node points and numerical subscripts refer to cell sides in Figure 3.1. Each cell consists of streamwise faces (sides 1 & 3) and cross-stream faces (sides 2 & 4). On the latter, Δx is zero and we drop the corresponding terms from the equations.

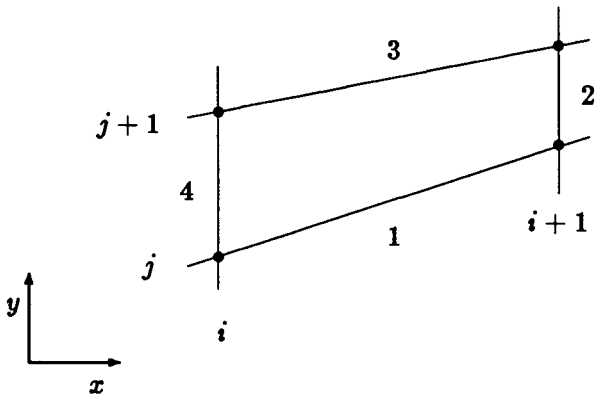

Figure 3.1: Computational Cell

Definition of Stream Function:

$$d\psi = \rho u dy_{x=const.}$$
$$\Delta\psi_2 - \rho_2 u_2 \Delta y_2 = 0$$

Conservation of Momentum:

$$\oint u d\psi + \oint P dy + \oint \tau dx = 0$$
$$u_1\Delta\psi_1 + u_2\Delta\psi_2 + u_3\Delta\psi_3 + u_4\Delta\psi_4$$
$$+P_1\Delta y_1 + P_2\Delta y_2 + P_3\Delta y_3 + P_4\Delta y_4$$
$$+\tau_1\Delta x_1 + \tau_3\Delta x_3 = 0$$

Conservation of Energy:

$$\oint H d\psi + \oint q dx = 0$$
$$H_1\Delta\psi_1 + H_2\Delta\psi_2 + H_3\Delta\psi_3 + H_4\Delta\psi_4 + q_1\Delta x_1 + q_3\Delta x_3 = 0 \tag{3.1}$$

Definition of Shear Stress:

$$\tau = (\mu_l + \mu_t)\partial u/\partial y$$
$$\tau_2\Delta y_2 - (\mu_l + \mu_t)_2\Delta u_2 = 0$$

Definition of Enthalpy Flux:

$$q = [\mu_l/Pr + \mu_t/Pr_t]\,\partial H/\partial y + \mu_{l_2}[1 - 1/Pr_l]\,u\partial u/\partial y$$
$$q_2\Delta y_2 - [\mu_l/Pr_l + \mu_t/Pr_t]_2\,\Delta H_2 - \mu_l[1 - 1/Pr]\,u_2\Delta u_2 = 0$$

In these equations, all "Δ " terms are simple centered differences in a counter-clockwise sense; e.g.

$$\begin{aligned} \Delta y_1 &= y_{i+1,j} - y_{i,j} \\ \Delta y_2 &= y_{i+1,j+1} - y_{i+1,j} \,. \end{aligned} \tag{3.2}$$

Cell side values of the functions are linear averages; e.g.

$$\begin{aligned} u_1 &= 0.5 \cdot (u_{i+1,j} + u_{i,j}) \\ u_2 &= 0.5 \cdot (u_{i+1,j+1} + u_{i+1,j}) \,. \end{aligned} \tag{3.3}$$

This discretization provides second order accurate approximations on an arbitrary grid. It preserves the conceptual simplicity of the governing equations, since each term in the discrete equations clearly is the flux of mass, momentum, or energy through a cell face. Since it is a Crank-Nicolson discretization, the solution is unconditionally stable for linear problems [Smith 78]. With all quantities given along line x_i, the above equations may be solved for quantities along x_{i+1} as discussed later.

Boundary Conditions

Boundary conditions are implemented very easily as part of the Newton solution procedure. Details of the inclusion of the boundary condition in the

Newton matrix will be discussed later. Note here, however, that the discrete equations above allow odd-even decoupling of the dependent variables, as do most central difference schemes for first derivatives. Thus, it is important that the boundary conditions be smoothly varying. To ensure some degree of smoothness, we assume boundary conditions are given at cell face midpoints and obtain the nodal values by averaging[1].

3.2 SIMILARITY AND GRID GENERATION

An effective boundary layer grid must follow the boundary layer growth. The outer edge of our grids is defined as $y_e(x) = \eta_\infty \cdot h(x)$. h is proportional to the boundary layer thickness δ, and we define the constant η_∞ so that $y_e > \delta$. Subsequent grid lines follow $y_j = \eta_j \cdot h_i$, where $\eta_j = \eta_{j-1} + \Delta\eta_j$, and the $\Delta\eta_j$ are chosen to give any desired spacing between the grid lines. We choose $h(x)$ to be the incompressible momentum thickness θ_k, since in most laminar and turbulent flows that quantity is proportional to the boundary layer thickness [Drela 83]. For similar flows, $\theta_k(x)$ is known from similarity principles. For non-similar flows, we calculate it as a part of the solution at each streamwise station.

3.2.1 Grid generation examples

The use of similarity principles for grid generation is best illustrated by examples. We begin by discussing grid requirements for flat plate and stagnation flows, and discuss grid generation for general similar and non-similar cases immediately afterwards.

Grid generation for flat plate and stagnation flow

The boundary layer thickness on a flat plate with sharp leading edge and constant edge velocity is zero at the leading edge and grows as $x^{1/2}$. The grid must follow this variation. Thus, we define $y_e = \eta_\infty x^{1/2}$ and generate the grid below. Because the equations are singular at $x = 0$, the grid begins arbitrarily close to $x = 0$, but not at $x = 0$.

A stagnation flow grid is particularly simple: the boundary layer thickness at a stagnation point is constant, giving a Cartesian grid.

[1]Note: This averaging does not in general preserve similarity. However, since real problems are nonsimilar, this is not a shortcoming. Alternatively, a logarithmic average could be taken, or, if the data is reasonably smooth, no averaging need be done.

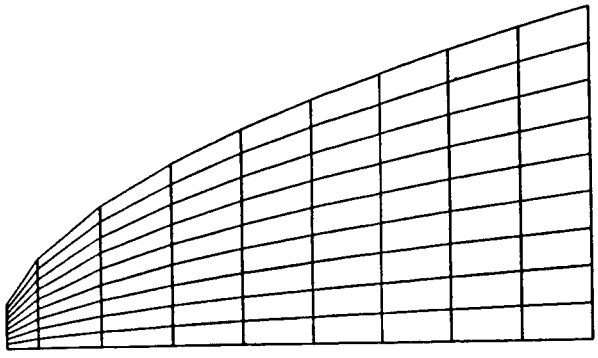

Figure 3.2: Computational grid for flat plate flow.

3.2.2 Grid generation for similar and non-similar flows

We discuss first the problem of generating a grid for any similar flow. Here the streamwise variation of θ_k is known *a priori* and grid generation is trivial. Subsequently, we discuss the process of calculating θ_k as part of the solution at each station, as a means of defining the grid in non-similar flows.

SIMILAR FLOWS

Grids generated for flat plate and stagnation flows are special cases of grids generated for similar flows. An incompressible flow is similar if the edge velocity varies as a power of x: $U_e \sim x^m$. This is the case in incompressible flows around a wedge. In similar flows, the variations of u, τ, ψ, H, and q along $\eta = const.$ are, by definition, functions of x only. All of these variables and δ follow a power law variation in x. Along $\eta = const.$ we can write:

$$u = x^{\alpha_u},\ \psi = x^{\alpha_\psi},\ \tau = x^{\alpha_\tau},\ H = x^{\alpha_H},\ q = x^{\alpha_q},\ \text{and}\ \delta = x^{\alpha} \qquad (3.4)$$

A similarity transformation of the differential forms of equations 2.1 - 2.5 readily yields the desired $\alpha's$[2]. If $\beta \cdot \pi$ is the wedge angle $(0 \leq \beta \leq 2)$, α is related to β via

$$\alpha = \frac{1-\beta}{2-\beta}, \qquad (3.5)$$

[2]Stagnation and flat plate flow have $\alpha_u (= m) = 1, 0$, respectively.

and

$$\begin{aligned} \alpha_u = \alpha_H &= 1 - 2\alpha \\ \alpha_\tau = \alpha_q &= 1 - 3\alpha \\ \alpha_\psi &= 1 - \alpha \end{aligned} \tag{3.6}$$

For similar flows, we are always given the edge velocity $U_e \sim x^{1-2\alpha}$. We can determine α from $U_e(x)$, define $\theta_{k_{i+1}} \sim \theta_{k_i}(x_{i+1}/x_i)^\alpha$, and generate our grid correspondingly.

NON-SIMILAR FLOWS

Method 1. Boundary layer flow is usually not similar. However, if streamwise changes are small, local regions of the flow may be locally similar. Method 1 assumes the local flow to be similar and estimates $\theta_{k_{i+1}}$, based on a calculated θ_{k_i} and a local value of α.

$$\theta_{k_{i+1}} = \theta_{k_i}\left[\frac{x_{i+1}}{x_i}\right]^{\alpha_i}. \tag{3.7}$$

This formula reduces to the previous treatment for similar flows, and gives a good approximation to θ_k for non-similar flows. However, if the boundary layer thickness grows more rapidly than the quasi-similar assumption predicts, we must allow the initial edge of the grid, y_e, to be far outside of the boundary layer, so that the boundary layer always remains within the computational domain.

Method 2. Instead of extrapolating to find $\theta_{k_{i+1}}$, this approach calculates $\theta_{k_{i+1}}$ at each station as a part of the solution. The grid ordinates $y_{i+1,j}$ are defined as $y_{i+1,j} = \eta_{i+1,j} \cdot \theta_{k_{i+1}}$, and $\theta_{k_{i+1}}$ is treated as an additional unknown in (2.15). To define θ_k and close equations 2.1 - 2.5 we must add an equation – the definition of θ_k – to equations 2.15. This process is discussed in more detail in Section 5.1.3.

3.3 STARTING THE SOLUTION

At any streamwise station, there are $J-1$ discrete control volumes, $2 \cdot J$ nodes (at i & $i+1$), and five unknowns per node, giving a total of $10 \cdot J$ unknowns. We want to solve 3.1 for the unknowns at station $i+1$. When the solution at i is known, the number of unknowns decreases to $5 \cdot J$. We can solve this system since, at each station, we have $5 \cdot (J-1)$ equations and 5 boundary conditions.

At $i = 0$, no previous solution is available, and we have only half the number of equations needed to solve for the unknowns. Somehow, we must generate a starting solution. Our approach is straightforward:

1. Assume the flow is similar between $i = 0$ and $i = 1$ and construct the grid accordingly.

2. Since, in similar flow, each variable V varies like $V_{i+1} = V_i \cdot (x_{i+1}/x_i)^{\phi}$ along constant η, replace the unknowns at $y_{i+1,j}$ by those at $y_{i,j}$ with the appropriate x-scaling, thereby reducing the number of unknowns to $5 \cdot J$.

3. Calculate the terms in the discretized equation, as before.

Below is an example of the approach applied to incompressible flat plate flow. In flat plate flow $\alpha_u = 0$, $\alpha_\tau = -1/2$, and $\alpha_\psi = 1/2$. To start the solution we set at every η_j:

Substitutions			Fluxes	
$u_{i=1}$ =	$u_{i=0}$	$\Rightarrow$	u_1 =	$(u_{i=0} + u_{i=1})/2 = u_{i=0}$
$\psi_{i=1}$ =	$\psi_{i=0} \cdot (x_0/x_1)^{-1/2}$	$\Rightarrow$	ψ_1 =	$\psi_{i=0} \cdot (1 + (x_0/x_1)^{-1/2})/2$
$\tau_{i=1}$ =	$\tau_{i=0} \cdot (x_0/x_1)^{1/2}$	$\Rightarrow$	τ_1 =	$\tau_{i=0} \cdot (1 + (x_0/x_1)^{1/2})/2$
etc.		$\Rightarrow$	*etc.*	

(3.8)

Fluxes through faces 2 and 3 can be defined with similar relations. Now, the discretized equations are written in terms of $3 \cdot J$ variables at $i = 0$, only, and we can solve for the unknowns. The approach is valid for any similar flow if the exponent of (x_0/x_1) is replaced by the appropriate α from (3.6).

This substitution is equivalent to using our exact knowledge of $\partial/\partial x$ ($\eta = const.$) to eliminate all streamwise derivatives and to solve the ordinary differential equation in η. The key to the procedure is our grid. Since the grid lines are generated to follow lines of constant η, the above substitution is justified. Transformation of the equations to similarity form is not necessary.

3.3.1 "True" Similarity Solutions

The use of similarity allows easy calculation of a starting solution. However, that solution is not, strictly speaking, a similarity solution. A true similarity solution, when scaled by η, must be independent of x. The above procedure uses a linear approximation to the streamwise variation of the

variables. This is an exact representation of the streamwise terms in stagnation point flows, where all variables are constant or vary linearly in x along $\eta = const.$ However, when the exponent $\alpha \neq 1,\ 0$ the streamwise variation is nonlinear and results in a second order truncation error. Thus the solution is dependent on x. The error may be eliminated by analytically integrating the streamwise terms (see Appendix A) since their streamwise variation is known in similar flows. This gives a true similarity solution. This correction is of primarily academic interest, however, since the error is very small and flows of interest are necessarily non-similar.

Chapter 4

ANALYSIS AND COMPARISON

This chapter compares and contrasts two aspects of the finite volume and conventional approaches:

- explicit versus implicit application of similarity concepts, and
- conservative versus non-conservative formulations.

We present a derivation of the Falkner-Skan equation, a popular conventional approach, to focus our discussion.

4.1 CONVENTIONAL APPROACH

The conventional approach[1] applies the divergence theorem to the incompressible version of equations 2.15 to get the differential form of the governing equations, in so-called divergence form:

$$\frac{\partial u}{\partial x} + \frac{\partial v}{\partial y} = 0 \tag{4.1}$$

$$\frac{\partial}{\partial x}(u \cdot u + P) + \frac{\partial}{\partial y}(v \cdot u) = \nu \frac{\partial^2 u}{\partial y^2}. \tag{4.2}$$

The non-divergence, or non-conservative, form

$$u\frac{\partial u}{\partial x} + v\frac{\partial u}{\partial y} = U_e \frac{dU_e}{dx} + \nu \frac{\partial^2 u}{\partial y^2} \tag{4.3}$$

[1]The derivation in this section closely follows [Schlichting 68] (Ch. 8 & 9).

is obtained by differentiating the products in the momentum equation, introducing the Bernoulli equation, and simplifying. The continuity equation can be integrated by introducing a streamfunction:

$$u = \frac{\partial \psi}{\partial y} \qquad\qquad v = -\frac{\partial \psi}{\partial x}. \tag{4.4}$$

Introducing (4.4) into equation 4.3 gives

$$\frac{\partial \psi}{\partial y}\frac{\partial^2 \psi}{\partial x \partial y} - \frac{\partial \psi}{\partial x}\frac{\partial^2 \psi}{\partial y^2} = U_e \frac{dU_e}{dx} + \nu \frac{\partial^3 \psi}{\partial y^3}. \tag{4.5}$$

The continuity equation has been eliminated at the cost of raising the order of the governing PDE by one.

Equation 4.5 can be cast in similarity form by application of one of a number of possible similarity transformations[2]. The Falkner-Skan transformation employs independent variables ξ and η

$$\xi = \frac{x}{L}\,, \qquad\qquad \eta = y\frac{\sqrt{R}}{Lg(x)}\,, \tag{4.6}$$

and a dimensionless stream function

$$f(\xi, \eta) = \psi(x, y)\frac{\sqrt{R}}{LU_e(x)g(x)}\,. \tag{4.7}$$

R is a Reynolds number, and L is a reference length. The scale factor $g(x)$ will be determined later.

Introduction of (4.6) and (4.7) into the momentum equation 4.5 yields, after some algebra, the governing third order PDE for boundary layer flow:

$$f_{\eta\eta\eta} + \alpha f f_{\eta\eta} + \beta(1 - f_\eta^2) = \frac{U_e}{U_\infty} g^2 \left[f_\eta \frac{\partial f_\eta}{\partial \xi} - f_{\eta\eta}\frac{\partial f}{\partial \xi} \right] \tag{4.8}$$

where α and β are:

$$\alpha = \frac{Lg}{U_\infty}\frac{d}{dx}(U_e g), \qquad \beta = \frac{L}{U_\infty} g^2 \frac{d}{dx} U_e\,. \tag{4.9}$$

Equation 4.8 is the counterpart of the incompressible form of equations 2.15, and is the starting point of many conventional numerical analyses[3].

[2] We show later that a valid similarity transformation for the boundary layer equations must reduce to one general form.

[3] Most numerical approaches now take the somewhat circuitous route to convert (4.8) *back* into a system of three first order PDE's in ξ and η before discretization and solution.

Similar solutions to equation 4.8 exist if f, f_η, and α and β do not depend on x. Then the right hand side of (4.8) vanishes and an ODE in η remains on the left hand side. The constraint on α and β gives two equations for the edge velocity and the scale factor. After some algebra one obtains

$$g = \sqrt{\frac{2}{m+1}\frac{x}{L}\frac{U_\infty}{U_e}}\,, \tag{4.10}$$

and

$$U_e = C \cdot x^m\,. \tag{4.11}$$

Potential velocity distributions with this form are found in wedge flows.

4.2 EFFECT OF SIMILARITY

If $U_e = Cx^m$, the flow is similar and equation 4.8 reduces to an ODE, allowing straightforward calculation of a starting solution. Although the finite volume approach uses no transformation, similarity principles can be used to start the solution. The two sections below discuss the parallels between the two approaches. For the purposes of this analysis, constant factors may be ignored.

4.2.1 Conventional Approach

For similar flows the scale factor g is

$$\begin{aligned} g &= \sqrt{\frac{2}{m+1}\frac{x}{L}\frac{U_\infty}{Cx^m}} \\ &= \sqrt{\frac{2U_\infty}{(m+1)CL}}x^{(1-m)/2}\,. \end{aligned} \tag{4.12}$$

Thus, the independent variable η becomes

$$\begin{aligned} \eta &= y\sqrt{\frac{m+1}{2}\frac{C}{\nu}}x^{(m-1)/2} \\ &= \frac{C_\eta y}{x^{(1-m)/2}} \end{aligned} \tag{4.13}$$

(C_η = constant), and the dependent variables are

$$\psi(x,y) = \sqrt{\frac{2}{m+1}}\sqrt{\eta C}x^{(m+1)/2}\,f(\eta) \tag{4.14}$$

$$u(x,y) = Cx^m f'(\eta) \tag{4.15}$$

$$v(x,y) = -\sqrt{\frac{m+1}{2}\eta C}x^{(m-1)/2}\left[f + \frac{m-1}{m+1}\eta\frac{\partial f}{\partial \eta}\right] . \tag{4.16}$$

Thus, in similar flow the stream function and the velocity components[4] are known functions (up to a constant multiplicative factor) of x along $\eta = const.$

The "character" of the Falkner-Skan transformation becomes clear if we consider the dependent variables 4.14 - 4.16 for constant η. Then, the relations become

$$\begin{aligned} \psi(x) &= C_\psi x^{(m+1)/2} \\ u(x) &= C_u x^m \\ v(x) &= C_v x^{(m-1)/2} . \end{aligned} \tag{4.17}$$

where C_ψ, C_u, and C_v depend on η. The streamwise and normal velocities are of no immediate interest since they are eliminated by the stream function. Consider the transformed streamfunction, however. From equation 4.7

$$f(\xi,\eta) = \psi(x,y)\frac{\sqrt{R}}{LU_e(x)g(x)} .$$

Inserting the definitions for U_e and $g(x)$ gives

$$f(\xi,\eta) = \psi(x,y)\frac{\sqrt{R}}{LCx^m\sqrt{\frac{2U_\infty}{(m+1)LC}}x^{(1-m)/2}} , \tag{4.18}$$

or

$$f(\xi,\eta) = \frac{\psi(x,y)}{C_f x^{(m+1)/2}} . \tag{4.19}$$

Comparison with equation 4.17 shows that, in similar flow, $f = const.$ along constant η. This certainly is not surprising. It is the crux of the similarity transformation. If it were not the case, equation 4.8 would not reduce to an ODE in η – the solution would not be similar.

Any number of similarity transformations are possible (and a large number have appeared in the literature). However, for similar flows they must have two points in common:

1. The ordinate must scale as $g(x)$.

[4]Note that the normal velocity in the conventional approach is defined by an ODE in η.

2. The transformed variables along any $\eta = const.$ line must be constant.

Thus, the transformed variables (') must be of the form (from (4.17))

$$\begin{aligned} \psi' &\sim \frac{\psi}{x^{(m+1)/2}} \\ u' &\sim \frac{u}{x^m} \\ v' &\sim \frac{v}{x^{(m-1)/2}} \end{aligned} \tag{4.20}$$

In this limited sense, similarity transformations of the incompressible boundary layer equations differ only in the degree of complexity that hides (4.17).

A noteworthy transformation in this regard is that due to Drela [Drela 83]. Drela writes the governing equations in first order form and transforms each primitive variable individually by the appropriate combination of U_e and $g(x)$. For example, $u' = u/U_e$ and $\psi' = \psi/(U_e g(x))$. In similar flow, $U_e \sim x^m$, $U_e g(x) \sim x^{(1+m)/2}$, etc. and his governing equations reduce to ODE's, as they must. His approach is one step towards simplifyng the governing equations – each transformed equation still represents a conservation law. However, the transformations and manipulations are still involved, the number of terms per equation is increased, and each term does not have a physical meaning.

4.2.2 Finite Volume Approach

The finite volume approach leaves the equations intact; rather, the grid is scaled to adapt to the flow. The normal location of the grid lines lie along $y = \eta h(x)$. With $h(x)$ defined as the incompressible momentum thickness, $h(x)$ is equivalent to $g(x)$ since in similar flow $\theta_k \sim \delta \sim x^{(m-1)/2}$ (cf. eqn. 4.12).

Having defined a computational mesh with grid lines that lie along constant η, each of the similarity relations 4.17 holds true. To calculate a starting solution, we express the variables at the unknown upstream station in terms of the values at the assumed known station (see Sec. 3.3), and apply the Newton procedure until convergence. In effect, the discrete PDE's reduce to ordinary *difference* equations.

The conventional and finite volume approaches can be thought of as, respectively, applying similarity principles explicitly (by transforming the equations) and implicitly (by scaling the grid). The grid scaling in the finite volume approach is functionally equivalent to the similarity transformation used in conventional schemes but is much simpler.

4.3 CONSERVATION

Conservation of mass, momentum, and energy means that in the discrete approximation to conservation equations, no spurious mass, momentum, or energy is created. Conserving mass, momentum, and energy is probably not mandatory in the subsonic region of the boundary layer, but is nevertheless a good feature. However, shocks may penetrate the essentially inviscid region near $y = y_e$, and strict conservation there may be essential for accurate prediction of shock strength and location. Conservation is one feature of the finite volume approach; however, conservation can not be shown for the discrete approximation to the transformed governing equation 4.8.

The finite volume method approximates the integral conservation form of the boundary layer equations on finite grid cells. The laws of conservation of mass, momentum, and energy are approximated by summing the fluxes of those quantities into and out of each cell. If one takes a line integral of the fluxes around an arbitrary number of cells, or, equivalently, sums the line integrals of each of the enclosed cells, the only contribution to that integral is due to fluxes through faces at the boundary of our contour. The fluxes on the inside of the contours cancel, since the fluxes leaving each cell are just those entering the surrounding cells, and every flux is accounted for.

Differential forms of the governing equations can be shown to be conservative if they can be written in the divergence form

$$\frac{\partial G}{\partial x} + \frac{\partial F}{\partial y} = 0. \tag{4.21}$$

and if the equations are discretized consistently. To show this, we simply apply the divergence theorem to equation 4.21 and obtain (assuming counter-clockwise integration)

$$\oint F dy - \oint G dx = 0 , \tag{4.22}$$

and show conservation as outlined above.

Equations 4.1, 4.2, and 4.21 are in this form; however, equation 4.8 is not. Since there seems to be no direct means of writing (4.8) in divergence form, we can not show discretizations based on (4.8) to be conservative.

Chapter 5

LINEARIZATION AND SOLUTION

This chapter discusses linearization of difference equations 3.1 and solution of the resulting matrix of linear equations with Newton's method. Because of the compact nature of the discretization in Section 3.1 the linearized system of equations forms a block tridiagonal matrix which can be inverted very efficiently. Sections 5.2 and 5.3 discuss the setup and inversion of this block matrix. Section 5.2 also generalizes the right hand side of this matrix equation to include global unknowns, which allow us to treat a variety of boundary conditions easily.

Much of the material on linearization, matrix inversion, and treatment of arbitrary boundary conditions is discussed in bits and pieces elsewhere. We present it here for the sake of completeness.

5.1 NEWTON LINEARIZATION

Equations 2.15 and their discretized counterparts 3.1 are a non-linear system of equations. Algebraic inversion to find the state variables is impossible. Instead, we apply Newton's method: we linearize the non-linear system, and invert the resulting linear system successively until equations 3.1 are identically satisfied. We review a one-dimensional application of this method briefly, to motivate its extension to multi-dimensions.

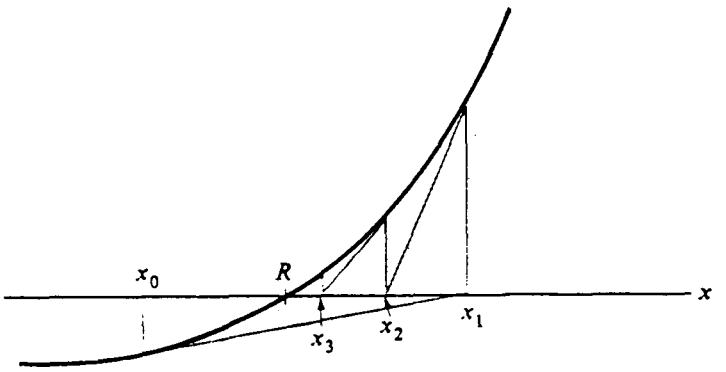

Figure 5.1: Newton Iteration in 1-Dimension

5.1.1 Rootfinding in 1-Dimension

In one dimension, we have a scalar function $f = f(v)$, along with a test solution $v = v^o$. In general $f(v^o) \neq 0$, therefore we seek a root v^i so that $f(v^i) = 0$. Newton's method constructs the truncated, two term Taylor series:

$$f(v) = 0 = f(v^o) + f'(v^o)\Delta v, \tag{5.1}$$

for $f(v)$, about v^o. Subsequent approximations v^{i+1} are found from $v^{i+1} = v^i + \Delta v$, where, from (5.1),

$$\Delta v = v^1 - v^0 = -\frac{f(v^o)}{f'(v^o)} \tag{5.2}$$

Geometrically, this process consists of calculating the tangent of f at $f(v^i)$, and sliding down it to v^{i+1} (see Fig. 5.1). We repeat the process until Δv is smaller than some predetermined value.

If f is well behaved, and we are far from local maxima or minima, each iteration gives a much improved value of v; therefore, we quickly converge to the solution. If $f(v)$ is a linear function of v, $f' = const.$ and one application of formula 5.2 *immediately* yields the desired result. If, however, $f(v)$ has local maxima or minima near v, $f'(v) \simeq 0$ and the algorithm fails spectacularly.

5.1.2 Rootfinding in N-Dimensions

The extension of Newton's method from 1 to J-dimensions is conceptually straightforward. Now we search for the solution *vector* $\mathbf{V}$ for the *system*

of equations $\mathbf{F(V)} = 0$. Instead of a single Taylor series expansion in one variable, J expansions in J variables are required for a *vector* of unknowns $\Delta\mathbf{V}$. Instead of the ordinary derivative f', we calculate $J \times J$ *partial* derivatives, $\partial f_i/dv_j i, j = 1 \cdots J$, and f can depend directly or *indirectly* on $\mathbf{V}$. This results in the system of J equations, below:

$$\begin{aligned}
f_1(\mathbf{V}) = 0 &= f_1(\mathbf{V}^i) + \tfrac{\partial f_1}{\partial v_1}\Delta v_1 + \tfrac{\partial f_1}{\partial v_2}\Delta v_2 + \tfrac{\partial f_1}{\partial v_3}\Delta v_3 + \ldots \\
f_2(\mathbf{V}) = 0 &= f_2(\mathbf{V}^i) + \tfrac{\partial f_2}{\partial v_1}\Delta v_1 + \tfrac{\partial f_2}{\partial v_2}\Delta v_2 + \tfrac{\partial f_2}{\partial v_3}\Delta v_3 + \ldots \\
f_3(\mathbf{V}) = 0 &= f_3(\mathbf{V}^i) + \tfrac{\partial f_3}{\partial v_1}\Delta v_1 + \tfrac{\partial f_3}{\partial v_2}\Delta v_2 + \tfrac{\partial f_3}{\partial v_3}\Delta v_3 + \ldots \\
&\vdots \\
f_J(\mathbf{V}) = 0 &= f_J(\mathbf{V}^i) + \tfrac{\partial f_J}{\partial v_1}\Delta v_1 + \tfrac{\partial f_J}{\partial v_2}\Delta v_2 + \tfrac{\partial f_J}{\partial v_3}\Delta v_3 + \ldots + \tfrac{\partial f_J}{\partial v_J}\Delta v_J
\end{aligned} \tag{5.3}$$

The process of iteration is the same: calculate successive $\Delta\mathbf{V}'s$ and iterate to drive $\mathbf{F(V)} = 0$. However, instead of sliding down lines to get the v^i that gives the intersection of $f(v^i)$ with 0, we now slide along J dimensional planes (hyperplanes) in search of their intersection. Also, the $\Delta\mathbf{V}'s$ can no longer be found by simple division. Inversion of the system to find $\Delta\mathbf{V}$ is a major task and is discussed in Section 5.3. Systems of specific interest to us are given below.

Incompressible laminar boundary layer flow In incompressible flow there are three equations in three unknowns at each cell j, giving (for $J-1$ cells) a system of $3(J-1)$ equations in $3J$ unknowns[1]. The resulting linear system for cell j is

$$\begin{aligned}
R_{m_j}(\mathbf{V}) = 0 = R_{m_j}(\mathbf{V}^i) + \tfrac{\partial R_{m_j}}{\partial u_j}\Delta u_j + \tfrac{\partial R_{m_j}}{\partial \psi_j}\Delta \psi_j + \tfrac{\partial R_{m_j}}{\partial \tau_j}\Delta \tau_j + (\ldots.)_{j+1} \\
R_{\psi_j}(\mathbf{V}) = 0 = R_{\psi_j}(\mathbf{V}^i) + \tfrac{\partial R_{\psi_j}}{\partial u_j}\Delta u_j + \tfrac{\partial R_{\psi_j}}{\partial \psi_j}\Delta \psi_j + \tfrac{\partial R_{\psi_j}}{\partial \tau_j}\Delta \tau_j + (\ldots.)_{j+1} \\
R_{\tau_j}(\mathbf{V}) = 0 = R_{\tau_j}(\mathbf{V}^i) + \tfrac{\partial R_{\tau_j}}{\partial u_j}\Delta u_j + \tfrac{\partial R_{\tau_j}}{\partial \psi_j}\Delta \psi_j + \tfrac{\partial R_{\tau_j}}{\partial \tau_j}\Delta \tau_j + (\ldots.)_{j+1}
\end{aligned} \tag{5.4}$$

R_{m_j}, R_{ψ_j}, and R_{τ_j} are the residuals of the momentum equation, and the definitions of stream function and shear stress, respectively (equations 3.1). The unknowns are $\Delta\mathbf{V} = [\Delta u\ \Delta\psi\ \Delta\tau\ ]^T$ at j and $j+1$. $\mathbf{V}^o$ is the vector of initial guesses.

[1] If the solution at i is known, each residual 3.1 depends on u, ψ, and τ at $(i+1, j)$ and $(i+1, j+1)$. However, the unknowns are shared by adjacent cells leading to a total of $3J$ variables. Three boundary conditions must be specified for closure.

Compressible turbulent boundary layer flow In compressible flow, there are five dependent variables, and we linearize the five discretized equations with respect to $\mathbf{V} = [u\ \psi\ \tau\ H\ q\ ]^T$. For compressible and turbulent flows the residuals are implicit as well as explicit functions of $\mathbf{V}$. This dual dependence of the residuals on $\mathbf{V}$ must be accounted for by applying the chain rule of differentiation when appropriate.

For example, the residual of the stream function for compressible depends on u and ψ explicitly, and on u *and* H implicitly. The implicit dependence is due to the equation of state:

$$\rho = \frac{\gamma}{\gamma - 1} \frac{P}{H - \frac{1}{2}u^2} \,. \tag{5.5}$$

Application of the chain rule gives (for a given P)

$$\begin{aligned} \frac{\partial R}{\partial u} &= \frac{\partial R}{\partial \rho}\frac{\partial \rho}{\partial u} = \frac{\partial R}{\partial \rho}\frac{\gamma}{\gamma - 1}\frac{P}{\left(H - \frac{1}{2}u^2\right)^2}u \\ \frac{\partial R}{\partial H} &= \frac{\partial R}{\partial \rho}\frac{\partial \rho}{\partial H} = \frac{\partial R}{\partial \rho}\frac{\gamma}{\gamma - 1}\frac{-P}{\left(H - \frac{1}{2}u^2\right)^2} \end{aligned} \tag{5.6}$$

Similar cross-differentiation should be performed for all implicit functions of u, τ, ψ, H, and q to ensure quadratic convergence of the Newton algorithm.

The cost of neglecting the variation of any quantity is high. Figure 5.2 shows the number of iterations needed for convergence when turbulent viscosity terms are linearized and not linearized. For higher Reynolds numbers, each station will require even more iterations.

5.1.3 Global unknowns

It is advantageous to include in the set of variables two global unknowns, $\Delta\theta_k$ and ΔU_e. We refer to $\Delta\theta_k$ and ΔU_e as global unknowns because they are unknown quantities that are functions of x only, and do not vary across the boundary layer. By allowing $\Delta\theta_k$ to be an unknown, we calculate the grid as part of the solution at each station ($y_{i,j} \equiv \eta_j \theta_{k_i}$). U_e usually *is* known *a priori*, and $\Delta U_e = 0$. However, in inverse calculations a quantity other than U_e is specified and ΔU_e must be treated as an unknown.

The global unknowns add two terms to each of equations 5.3,

$$\frac{\partial R}{\partial \theta_k}\Delta\theta_k \qquad \text{and} \qquad \frac{\partial R}{\partial U_e}\Delta U_e \,. \tag{5.7}$$

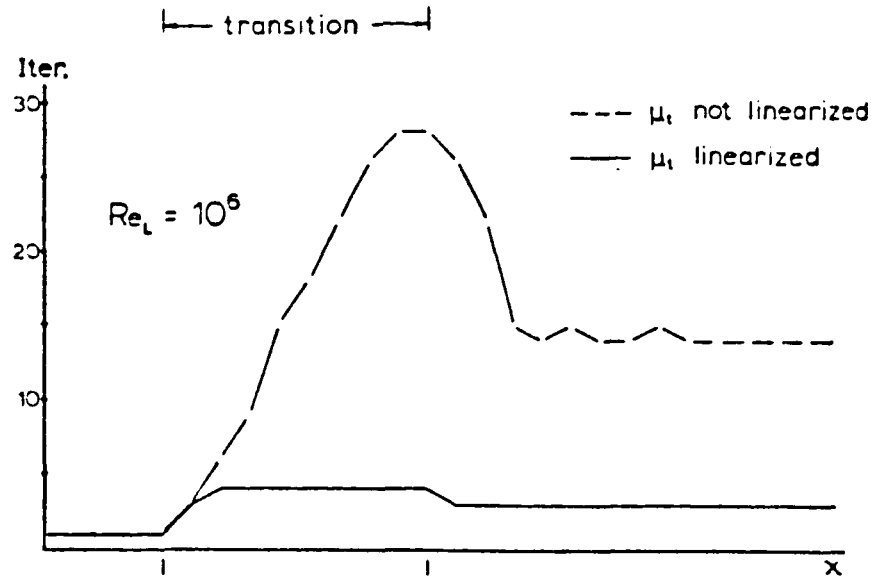

Figure 5.2: Effect of linearizing eddy viscosity on number of iterations per streamwise station.

Although these terms are added at each cell, the total number of variables increases by only two since $\Delta\theta_k$ and ΔU_e are constant in the cross-stream direction. Two corresponding relations must be introduced to close the system of equations. The (incompressible) definition of θ_k,

$$\theta_k = \int_0^{y_\infty} \frac{u}{U_e}\left(1 - \frac{u}{U_e}\right) dy \,, \tag{5.8}$$

upon discretization gives one relation. The second must be derived from the fifth specified boundary condition. If U_e is specified,

$$\Delta U_e = U_{spec} - U_e \tag{5.9}$$

is sufficient. If some other (inverse) boundary condition is specified, the form of (5.9) must be derived from the definition of that boundary condition (see Appendix D).

The turbulence model contains two additional global unknowns, velocity defect Δ_u and shear velocity U_τ. For simplicity, we do not treat them as such. In effect, this causes the influence of their variation on the residual to lag by one iteration, and the convergence rate may decrease. However, the velocity defect typically varies slowly from station to station; thus, neglecting its variation has little effect on the convergence rate. The global changes in the shear velocity can be adequately modeled by the local variations in shear stress and density since $U_\tau = f(\tau_w, \rho_w)$ and $\tau_w \simeq \tau_j$, $\rho_w \simeq \rho_j$ in the inner layer.

5.1.4 Boundary Conditions

Applying the Newton method to the set of five equations over $J-1$ cells gives a set of $5\cdot(J-1)$ linear equations (5.3) at each streamwise station, for $5\cdot J+2$ variables (if the solution at the previous station is known). The two auxillary relations and five boundary conditions supply the equations needed for closure. The boundary conditions are implemented by initializing the applicable state variable to its boundary value, and requiring all subsequent changes to that variable be zero. This gives five relations of the form

$$\Delta u^n_{1,i} = 0 \tag{5.10}$$

(the no slip condition in this example) that close the system.

5.2 BLOCK MATRIX SETUP

The system of equations 5.3 is complete when boundary conditions, global unknowns, and auxillary relations are included. With two global unknowns, a computational region of $J-1$ cells results in a $(5J+2)\times(5J+2)$ matrix:

$$\begin{bmatrix} A_1 & C_1 & & & \mathbf{G_1} & \mathbf{H_1} \\ B_2 & A_2 & C_2 & & \mathbf{G_2} & \mathbf{H_2} \\ & \cdots & \cdots & \cdots & \cdots & \cdots \\ & & B_J & A_J & \mathbf{G_J} & \mathbf{H_J} \\ xx & xx & xx & xx & xx & xx \\ xx & xx & xx & xx & xx & xx \end{bmatrix} \begin{bmatrix} \mathbf{\Delta V_1} \\ \mathbf{\Delta V_2} \\ \cdot\cdot \\ \mathbf{\Delta V_J} \\ \Delta\theta_k \\ \Delta U_e \end{bmatrix} = \begin{bmatrix} \mathbf{R_1} \\ \mathbf{R_2} \\ \cdot\cdot \\ \mathbf{R_J} \\ R_{\theta_k} \\ R_{U_e} \end{bmatrix} \tag{5.11}$$

$\mathbf{\Delta V_j}$ is the vector of unknowns $[\Delta u\ \Delta\psi\ \Delta\tau\ \Delta H\ \Delta q\ ]^T_j$. A_j, B_j, and C_j are 5×5 matrices containing boundary condition terms and the derivatives $\partial R_j/\partial V_j$ and $\partial R_j/\partial V_{j+1}$. $\mathbf{R_j}$ is the negative of the vector of residuals of the five equations at cell j, while $\mathbf{G_j}$ and $\mathbf{H_j}$ are vectors containing $\partial\mathbf{R}_j/\partial\theta_k$ and $\partial\mathbf{R}_j/\partial U_e$, respectively. The $(J+1)$'th and $(J+2)$'th line each contains one scalar equation, the linearized momentum thickness (5.8) and (5.9) (or some other specified boundary condition), respectively. Derivation of these relations is discussed in Appendix D.

Due to the compact discretization, each residual depends only on variables at the neighboring node points and on the global unknowns. With imposition of the boundary conditions, the structure of the $5J\times 5J$ submatrix (*sans* global terms) is blocktridiagonal. One may take advantage of

this structure by transposing the columns containing the global terms to the right hand side of (5.11) and treating the global unknowns as quantities to be determined after inversion. The resulting matrix of equations is

$$\begin{bmatrix} A_1 & C_1 & & \\ B_2 & A_2 & C_2 & \\ & \cdots & \cdots & \cdots \\ & & B_J & A_J \end{bmatrix} \begin{bmatrix} \Delta\mathbf{V_1} \\ \Delta\mathbf{V_2} \\ .. \\ \Delta\mathbf{V_J} \end{bmatrix} = \begin{bmatrix} \mathbf{R_1} \\ \mathbf{R_2} \\ .. \\ \mathbf{R_J} \end{bmatrix} - \Delta\theta_k \begin{bmatrix} \mathbf{G_1} \\ \mathbf{G_2} \\ .. \\ \mathbf{G_J} \end{bmatrix} - \Delta U_e \begin{bmatrix} \mathbf{H_1} \\ \mathbf{H_2} \\ .. \\ \mathbf{H_J} \end{bmatrix} . \tag{5.12}$$

All matrices and vectors in equation 5.12 are listed in Appendix E. Equations $J+1$ and $J+2$ will be reintroduced after this system of equations is inverted.

5.3 BLOCK TRIDIAGONAL INVERSION

Solution of the block tridiagonal matrix is similar to solution of a scalar tridiagonal matrices. The algorithm is the same, with scalar operations replaced by matrix operations. At each iteration, we form the recurrence relations

$$\begin{aligned} D_1 &= A_1 \\ E_j &= [D_j^{-1}]C_j \qquad 1 \le j \le J \\ D_j &= A_j - [B_j]E_{j-i} \qquad 2 \le j \le J. \end{aligned} \tag{5.13}$$

For 3×3 blocks we form the inverse via Cramer's rule. This is inefficient for 5×5 blocks, where instead we factorize the matrices by Gauss elimination.

Applying the same operations to the right hand side gives

$$\begin{aligned} \mathbf{Z_1} &= [D_1^{-1}]\mathbf{R_1} \\ \mathbf{Z}_j &= [D_j^{-1}][\mathbf{R}_j - [B_j]\mathbf{Z}_{j-i}] \qquad 2 \le j \le J \\ \mathbf{Z1_1} &= [D_1^{-1}]\mathbf{G_1} \\ \mathbf{Z1}_j &= [D_j^{-1}[\mathbf{G}_j - [B_j]\mathbf{Z1}_{j-i}] \qquad 2 \le j \le J \\ \mathbf{Z2_1} &= [D_1^{-1}]\mathbf{H_1} \\ \mathbf{Z2}_j &= [D_j^{-1}[\mathbf{H}_j - [B_j]\mathbf{Z2}_{j-i}] \qquad 2 \le j \le J \end{aligned} \tag{5.14}$$

Combining left and right hand sides gives the intermediate result

$$\begin{bmatrix} I & E_1 & & \\ & I & E_2 & \\ & \cdots & \cdots & \cdots \\ & & & I \end{bmatrix} \begin{bmatrix} \Delta\mathbf{V_1} \\ \Delta\mathbf{V_2} \\ .. \\ \Delta\mathbf{V_J} \end{bmatrix} = \begin{bmatrix} \mathbf{Z_1} \\ \mathbf{Z_2} \\ .. \\ \mathbf{Z_J} \end{bmatrix} - \Delta\theta_k \begin{bmatrix} \mathbf{Z1_1} \\ \mathbf{Z1_2} \\ .. \\ \mathbf{Z1_J} \end{bmatrix} - \Delta U_e \begin{bmatrix} \mathbf{Z2_1} \\ \mathbf{Z2_2} \\ .. \\ \mathbf{Z2_J} \end{bmatrix} \tag{5.15}$$

where I is the identity matrix.

Finally, we eliminate the upper band of E matrices: subtract $E_{j-1}\times$ row j from row $j-1$ to get

$$\begin{bmatrix} \Delta\mathbf{V_1} \\ \Delta\mathbf{V_2} \\ .. \\ \Delta\mathbf{V_J} \end{bmatrix} = \begin{bmatrix} \mathbf{ZZ_1} \\ \mathbf{ZZ_2} \\ .. \\ \mathbf{ZZ_J} \end{bmatrix} - \Delta\theta_k \begin{bmatrix} \mathbf{ZZ1_1} \\ \mathbf{ZZ1_2} \\ .. \\ \mathbf{ZZ1_J} \end{bmatrix} - \Delta U_e \begin{bmatrix} \mathbf{ZZ2_1} \\ \mathbf{ZZ2_2} \\ .. \\ \mathbf{ZZ2_J} \end{bmatrix} \tag{5.16}$$

where, for example,

$$\begin{aligned} \mathbf{ZZ}_J &= \mathbf{Z}_J \\ \mathbf{ZZ}_{j-1} &= \mathbf{Z}_j - E_{j-1}\mathbf{ZZ}_j \qquad 2 \le j < J, \end{aligned} \tag{5.17}$$

etc.

At each j, we now have the scalar equations

$$\begin{aligned} \Delta u_j &= ZZ_{1,j} - \Delta\theta_k \cdot ZZ1_{1,j} - \Delta U_e \cdot ZZ2_{1,j} \\ \Delta\psi_j &= ZZ_{2,j} - \Delta\theta_k \cdot ZZ1_{2,j} - \Delta U_e \cdot ZZ2_{2,j} \\ \Delta\tau_j &= ZZ_{3,j} - \Delta\theta_k \cdot ZZ1_{3,j} - \Delta U_e \cdot ZZ2_{3,j} \\ \Delta H_j &= ZZ_{4,j} - \Delta\theta_k \cdot ZZ1_{4,j} - \Delta U_e \cdot ZZ2_{4,j} \\ \Delta q_j &= ZZ_{5,j} - \Delta\theta_k \cdot ZZ1_{5,j} - \Delta U_e \cdot ZZ2_{5,j} \end{aligned} \tag{5.18}$$

that must be solved for Δu_j, $\Delta\psi_j$, $\Delta\tau_j$, ΔH_j, and Δq_j. ZZ, $ZZ1$, and $ZZ2$ are known quantities. The two auxilliary relations determine $\Delta\theta_k$ and ΔU_e. We write them in the form

$$\begin{aligned} A_1\Delta\theta_k + B_1\Delta U_e &= R_1 \\ A_2\Delta\theta_k + B_2\Delta U_e &= R_2\,, \end{aligned} \tag{5.19}$$

(see Appendix D.2) calculate $\Delta\theta_k$ and ΔU_e using Cramer's rule, and, subsequently, calculate $\Delta\mathbf{V}_j$ for all j.

A convenient convergence criterion is the size of $(\Delta\mathbf{V}/\mathbf{V})_j$. If $max(\Delta\mathbf{V}/\mathbf{V})_j < \epsilon$, the Newton iteration has converged to a solution at that streamwise station. If not, we update $\mathbf{V}_j^{i+1} = \mathbf{V}_j^i - \Delta\mathbf{V}_j^i$ and repeat the process.

5.3.1 CPU Requirements

Solution of the block tridiagonal Newton matrix leads to very modest computer time requirements; especially, if the inversion procedure is optimized by taking zero columns and rows in each submatrix into account, For example, solution of the incompressible equations with the Cebeci-Smith turbulence model and 40 cells across the boundary layer takes approximately 0.12 seconds/iteration of CPU time on a *Digital Microvax* II[2]. Typically, 2−6

[2]Comparable to the *Digital VAX* 11/750

iterations are required for convergence. Thus, a turbulent test case with 50 stations and 40 cells across the boundary layer requires well under 30 seconds of CPU time on the *Microvax II*.

Chapter 6

RESULTS

The finite volume scheme (FVS) has been applied to a number of test cases with excellent results. We present several typical similar and non-similar test cases below. Results obtained for similar flows are compared to solutions obtained with Keller's Box Scheme (KBS) [Keller 70]. Non-similar results are compared to solutions obtained with the method of Drela[1] (DS) [Drela 83]. Results for turbulent flow cases are compared with experiment, and, in one case, with a previous solution.

6.1 SIMILAR FLOW

Similar flow, though of little practical interest, provides ideal test cases for comparison of the finite volume scheme with conventional methods. The flat plate non-dimensional wall shear stress

$$\frac{\tau_0}{\mu U_\infty}\sqrt{\frac{\nu x}{U_\infty}} \tag{6.1}$$

and displacement thickness

$$\delta^*\sqrt{\frac{U_\infty}{\nu x}} \tag{6.2}$$

values, with the percent error are given in Table 6.1. They have been calculated with KBS and FVS for various grid spacings[2]. The upper boundary

[1]Drela's method is a conventional (by our def.) second order accurate scheme that has been validated on a number of test cases.

[2]Solutions were "optimized" by *aposteriori* choice of the b ($b = \Delta\eta_{j+1}/\Delta\eta_j$) that gave the most accurate solution for each method and case with a ten cell base grid. Denser grids were generated by subdividing each base grid cell into equal intervals.

of the computational grid was set at

$$\eta_\infty = y\sqrt{\frac{U_\infty}{\nu x}} = 8 \tag{6.3}$$

for both schemes[3].

Table 6.1: Flat plate wall shear/*percent error:*

	WALL SHEAR		DISP. THICK.	
# cells	Keller	Fin. Vol.	Keller	FIN. Vol.
b	1.0	1.2	1.0	1.2
10	0.33085	0.33700	1.77121	1.69312
..	*0.363%*	*-1.488%*	*-2.932%*	*1.605%*
20	0.33177	0.33328	1.73342	1.71353
..	*0.087%*	*-0.368%*	*-0.787%*	*0.419%*
40	0.33199	0.33237	1.72393	1.71899
..	*0.022%*	*-0.092%*	*-0.185%*	*0.102%*
80	0.33204	0.33213	1.72156	1.72037
..	*0.006%*	*-0.023%*	*-0.047%*	*0.022%*
Exact	0.33206		1.72074	

KBS wall shear results are somewhat more accurate than FVS shear results, but the finite volume scheme predicts the displacement thickness slightly more accurately than does KBS. Both sets of results are extremely accurate, however, and the differences are minute. The errors for both schemes decrease as the square of the grid spacing, indicating second order accurate discretizations.

Table 6.2 gives the non-dimensional shear and displacement thickness for stagnation point flow as calculated by FVS and KBS. Definitions (6.1), (6.2), and (6.3), have been used with U_∞/x replaced by dU_e/dx and $\eta_\infty = 4$. The schemes predict the wall shear equally well, but FVS again gives more accurate displacement thicknesses. This might be expected from the basic formulation. The KBS approximates the differential equation and therefore gives greater accuracy for pointwise quantities. The FVS approximates the integral equations thus yielding greater accuracy of global quantities.

[3]Note: this η differs from the η in $\eta = y/\theta$ by a factor of 0.664

Table 6.2: Stag. point wall shear/*percent error:*

	WALL SHEAR		DISP. THICK.	
# cells	Keller	Fin. Vol.	Keller	FIN. Vol.
b	1.2	1.2	1.2	1.2
10	1.22733	1.237747	0.65871	0.64426
..	*0.427%*	*-0.418%*	*-1.666%*	*0.563%*
20	1.23126	1.23388	0.65059	0.64701
..	*0.108%*	*-0.105%*	*-0.414%*	*0.139%*
40	1.23226	1.23291	0.64853	0.64772
..	*0.027%*	*-0.026%*	*-0.095%*	*0.029%*
80	1.23251	1.23267	0.64801	0.64791
..	*0.007%*	*-0.007%*	*-0.015%*	*0.001%*
Exact	1.232588		0.64791	

6.2 NON-SIMILAR FLOW

6.2.1 Laminar Flow

Figure 6.1 shows the distribution of momentum thickness along an infinite cylinder as calculated by FVS and DS with the potential flow pressure distribution. Fifty points in the normal direction and $\Delta x = \pi/180$ were used. This test case is a good example of non-similar laminar flow around a blunt body. At small θ, u increases linearly and the flow approximates stagnation flow. After $\theta = 90^0$ the velocity decreases and the pressure gradient becomes positve; and, finally at $\theta = 106^0 - 109^0$, the flow separates.

The two curves are almost identical. In both cases, the solution diverged at $\theta = 107$ indicating separation of the flow. Figure 6.2 gives the corresponding wall shear stresses. Again, the curves are almost identical.

Howarth's flow is a popular, if artificial, laminar test case. It is defined by a linearly decreasing edge velocity: $U_e = 1 - x/8$. This definition gives a singular solution at $x = 0$, an increasingly positive pressure gradient at larger x, and separation at $x \simeq .96$. In this calculation there are 100 cross-stream points and $\Delta x = 0.01$. Figures 6.3 and 6.4 show the momentum thickness and wall shear stress, respectively. The curves are nearly indistinguishable away from the singular point. Both solutions fail to converge at $x = 0.965$, indicating separation at about $x = 0.96$ (the previous station is at 0.955). A

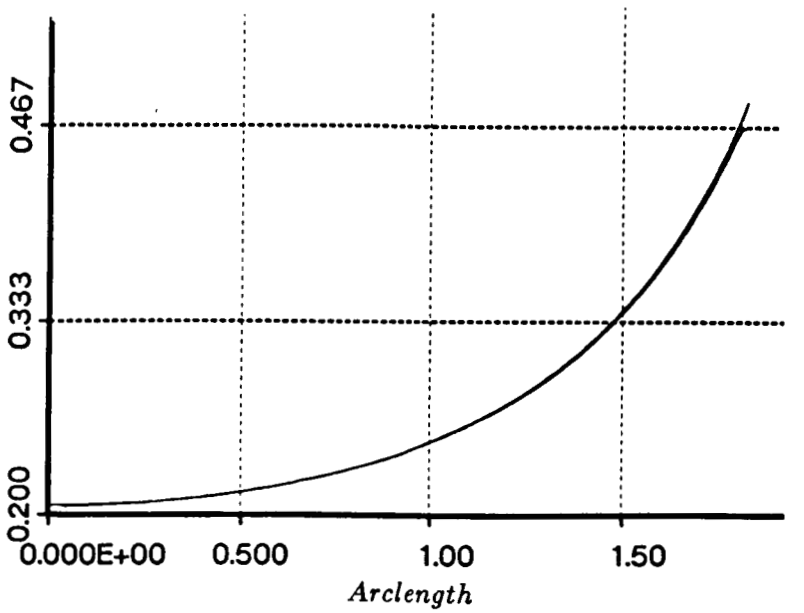

Figure 6.1: Momentum thickness on infinite cylinder

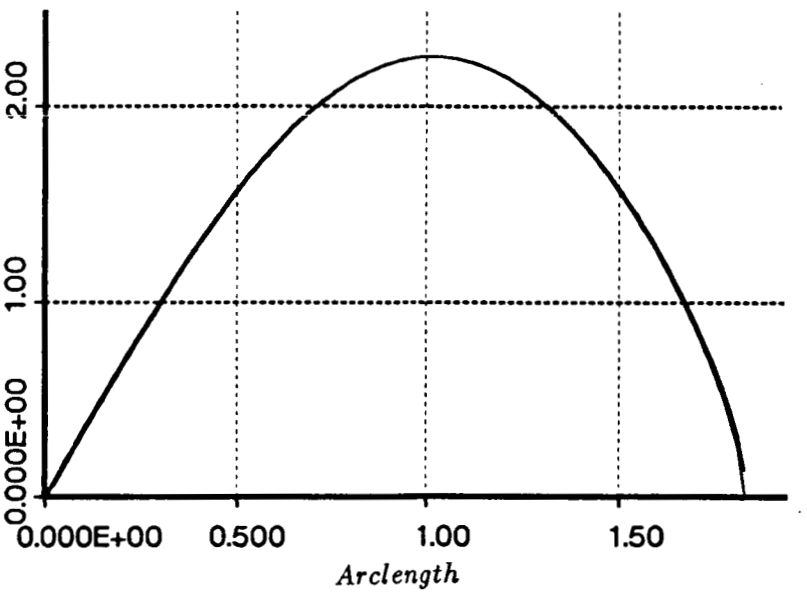

Figure 6.2: Wall shear on infinite cylinder

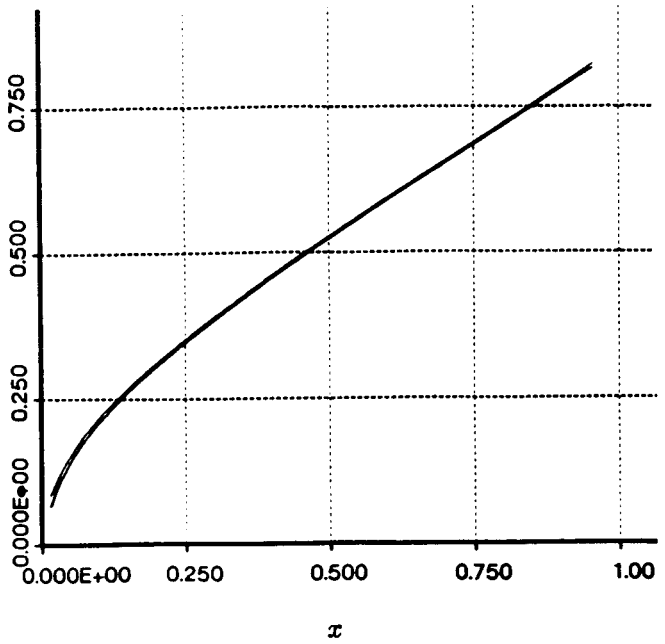

Figure 6.3: Momentum thickness in Howarth's flow

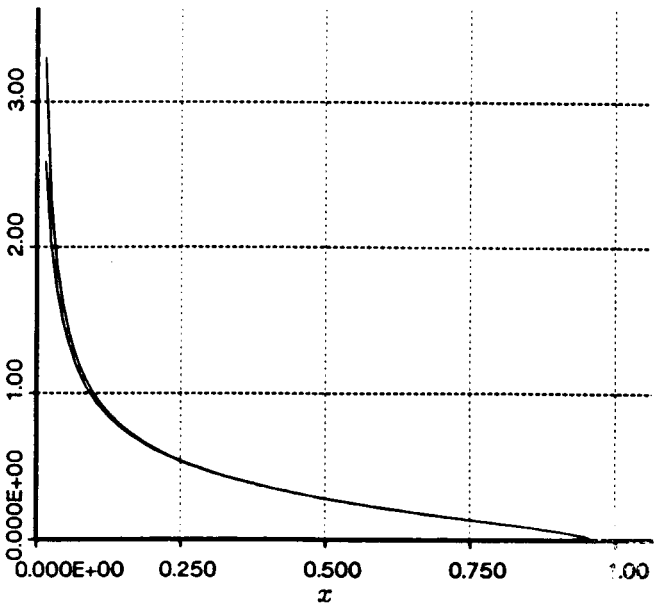

Figure 6.4: Wall shear in Howarth's flow

grid density study in [Loyd 85] showed no significant changes as the number of grid points was decreased to 25×25.

6.2.2 Turbulent Flow

Finally, we compare numerical results of two turbulent flow cases with experiment. The primary purpose of these test cases is to demonstrate the straightforward extension of the finite volume scheme to turbulent flows. As such, no attempt was made to "fine tune" the turbulence model or to "smooth" either input data or numerical results to attain better agreement with experiment.

In the following figures unconnected symbols represent either the experimental data or previous calculations, while connected symbols are the finite volume results. All test cases were run with 40 cells across the boundary layer and a stretching ratio $b = 1.15$.

Flows 2100 and 2400 from the 1968 Stanford Conference [Coles 69] are fully turbulent, and essentially incompressible. Initial conditions must be assumed to start the computations. A possible approach is to use the initial $U-$velocity profile data, integrate it to get the appropriate $\psi_{1,j}$, and input it to the turbulence model to calculate the apparent stresses and, subsequently, the shear stresses. However, this method is difficult to implement if few profile points are available, since interpolation is necessary and a suitable near wall model must be used. Instead, our approach has been very simple. We assume that the fully turbulent flow is "similar" in a small region near the first station, and choose the exponent in $U_e \sim x^{\alpha_*}$ to get the best possible agreement of the "similarity" solution with the data at the first station.

Flow 2100 is the boundary layer on a large airfoil-like body, at Reynolds number[4] $Re = 5.0 \cdot 10^5$. The edge velocity distribution is shown in Figure 6.5. The pressure gradient is negative at first, then nearly constant, and finally positive. The experimental data indicates the onset of separation at the final stations. Data is available at 38 streamwise stations, but at less than ten cross-stream data points near the leading edge. Calculation stations were taken at the locations of the experimental data.

Figure 6.6 shows the measured and calculated mean velocity profiles at the first three stations. The profiles were non-dimensionalized by the edge velocity at the first station. For clarity, the profiles have been plotted for $u/U_{e1} > 0.5$. The profiles at all three stations agree quite well with the

[4]Based on reference quantities at first station.

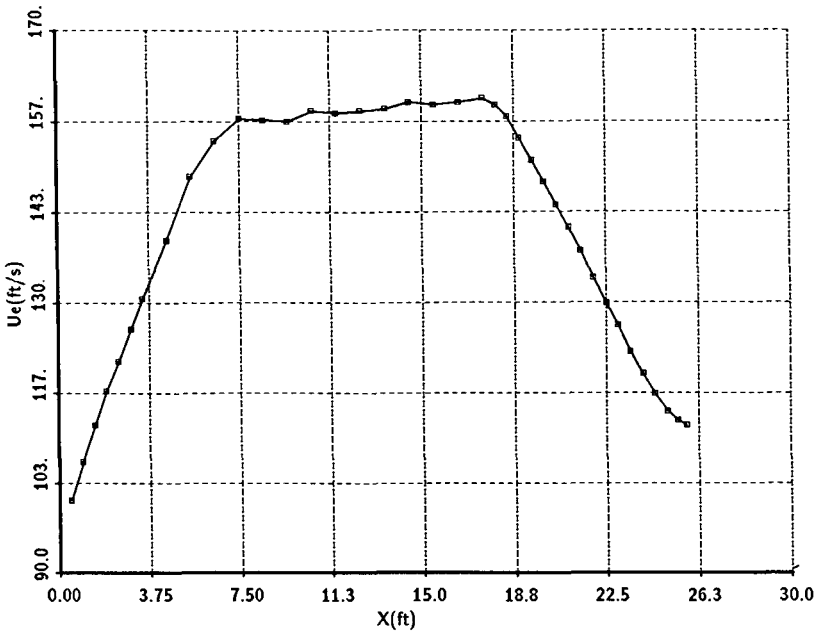

Figure 6.5: Flow 2100: Measured edge velocity

experimental data, thus validating the assumptions made in calculating the initial conditions.

Figure 6.7 gives the experimental and predicted skin friction coefficients for Flow 2100. The predicted values are in excellent agreement with the data for $x < 20ft$. For $x > 20ft$. (approaching separation) the computation overpredicts the skin friction.

The shape factor $H(x)$ is plotted in Figure 6.8, and the momentum thickness in Figure 6.9. Again, the trends and variations of the experiment are modeled well except near the separation point. Inability of the turbulence model to accurately predict the eddy viscosity near separation is the probable reason for this discrepancy.

Flow 2400 begins in a fairly strong positive pressure gradient, which abruptly decreases to zero (see Fig. 6.10). Extensive cross-stream data is available, but only 7 streamwise stations were measured. Twenty stations were used in the computation. The edge velocity at the intermediate stations was obtained by linear interpolation of the experimental data and is given in Figure 6.10. No attempt was made to smooth out the discontinuity in dU_e/dx.

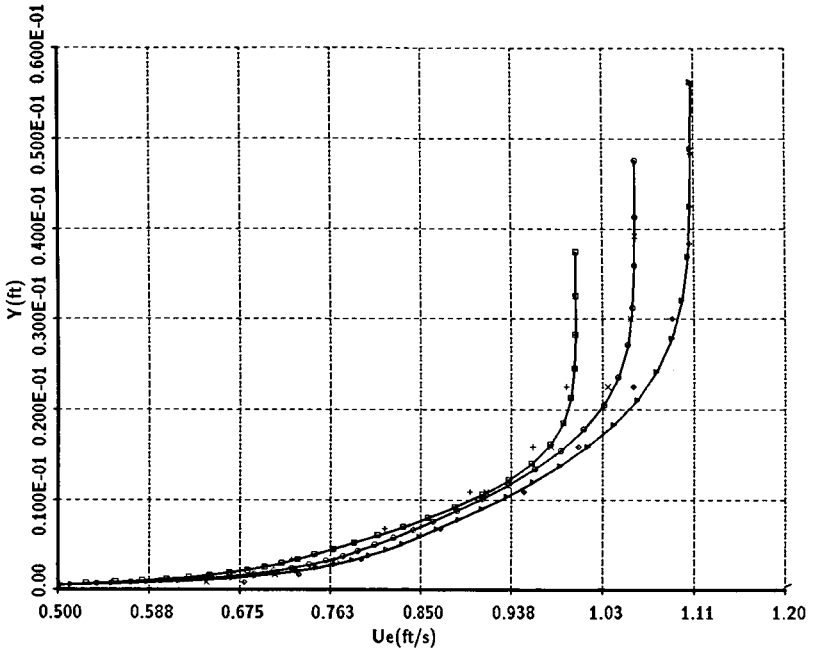

Figure 6.6: Flow 2100: Mean velocity profiles

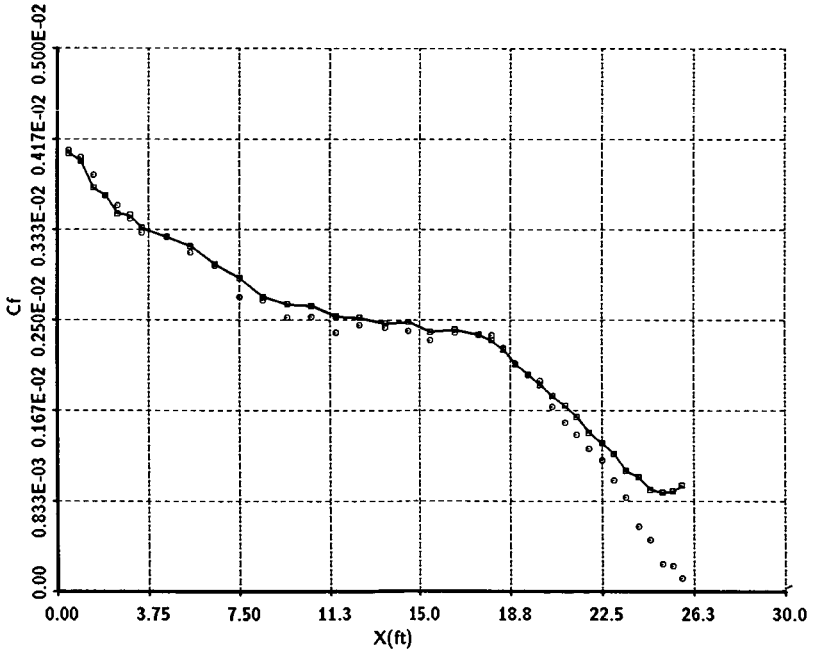

Figure 6.7: Flow 2100: Computed and experimental skin friction

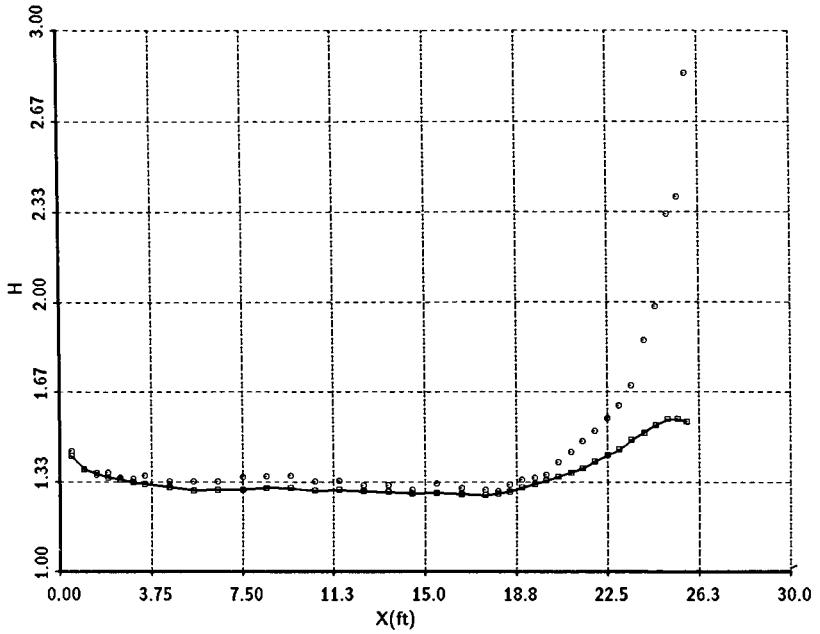

ψ Figure 6.8: Flow 2100: Computed and experimental H

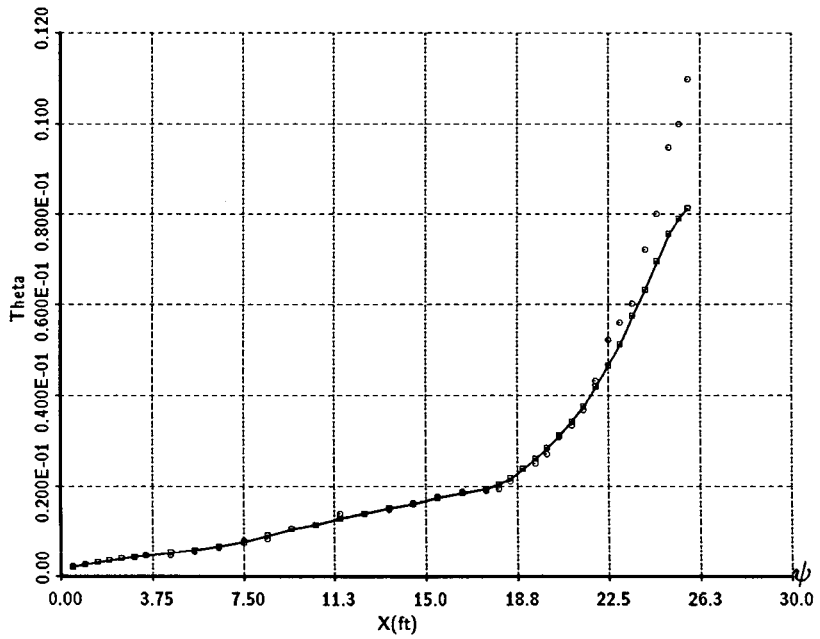

Figure 6.9: Flow 2100: Computed and experimental θ

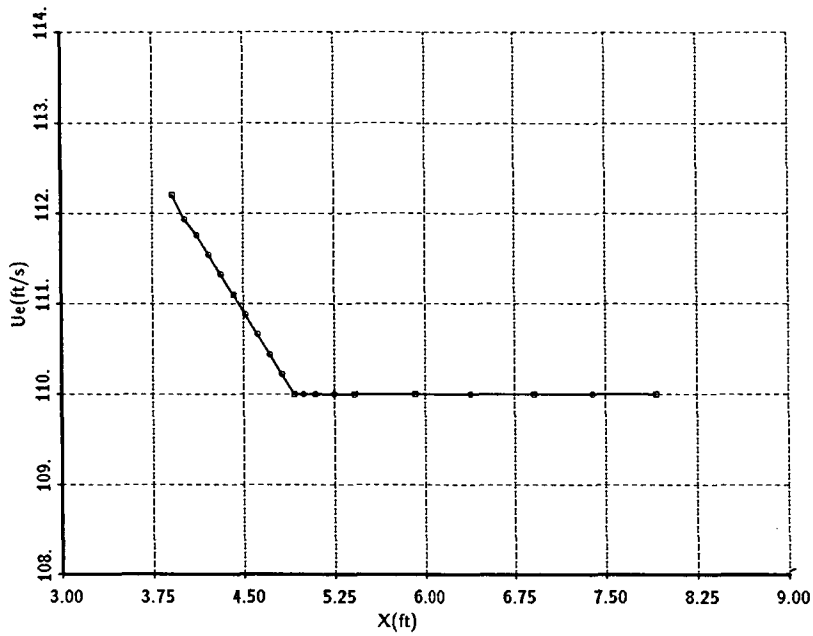

Figure 6.10: Flow 2400: Measured edge velocity

Due to the adverse pressure gradient the numerical results are very sensitive to the assumed power variation of U_e at the first station. Velocity profiles at the first three stations are shown in Figure 6.11. The agreement is not as good as in the previous case.

Figure 6.12 gives the predicted and measured skin friction distribution. A maximum error of approximately 10% is evident at the first and second stations. The influence of the initial conditions decreases as the solution marches downstream and the values of the predicted skin friction approach the experimental data.

Figures 6.13 and 6.14 show the shape factor and the momentum thickness, respectively. The magnitude of the error in the predicted values parallels that of the skin friction.

The results for turbulent flows are comparable in accuracy to finite difference calculations in [Coles 68] computed with the Cebeci-Smith turbulence model. In the present study we have attempted only to show that a finite volume method is as accurate as corresponding finite difference methods. We have not attempted to improve the turbulence model.

Finally we present results for a compressible flow case. It is the tur-

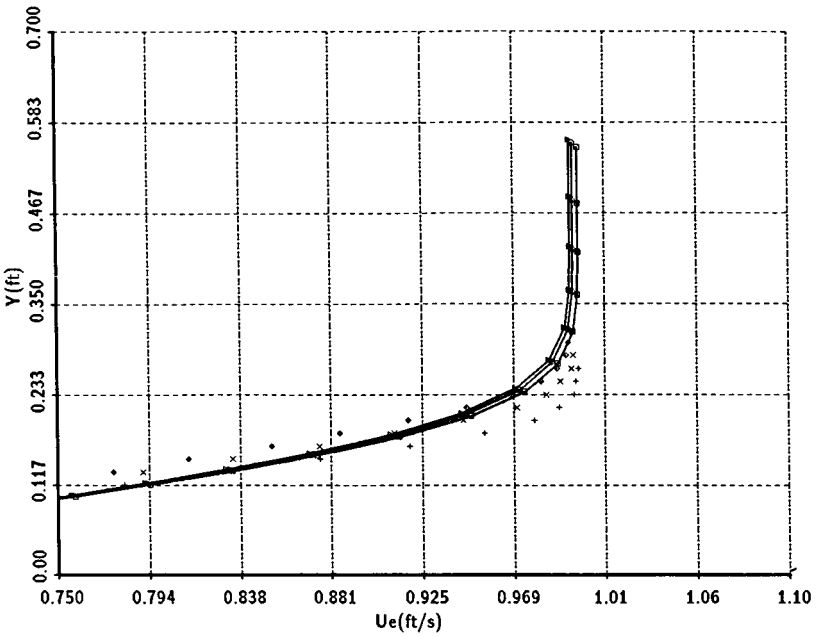

Figure 6.11: Flow 2400: Mean velocity profiles

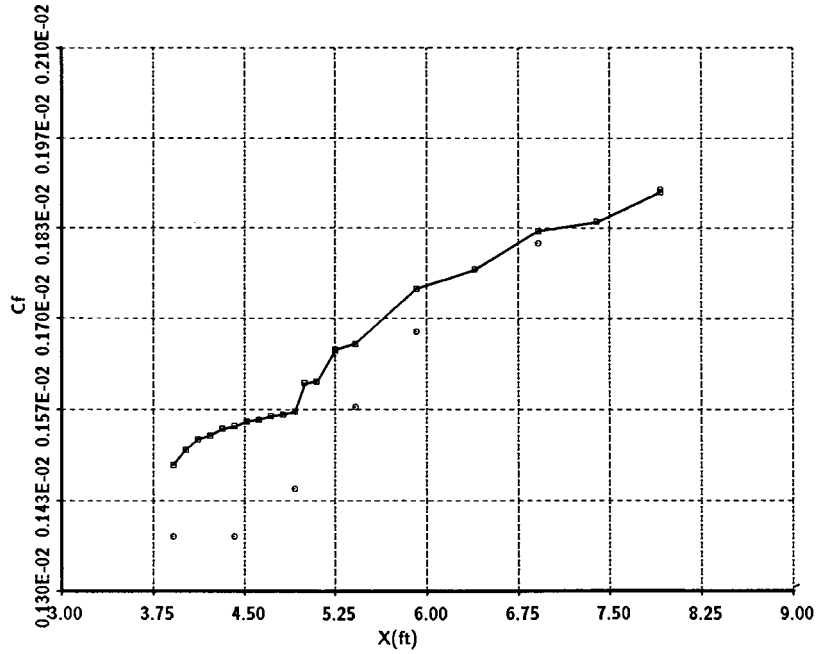

Figure 6.12: Flow 2400: Computed and experimental skin friction

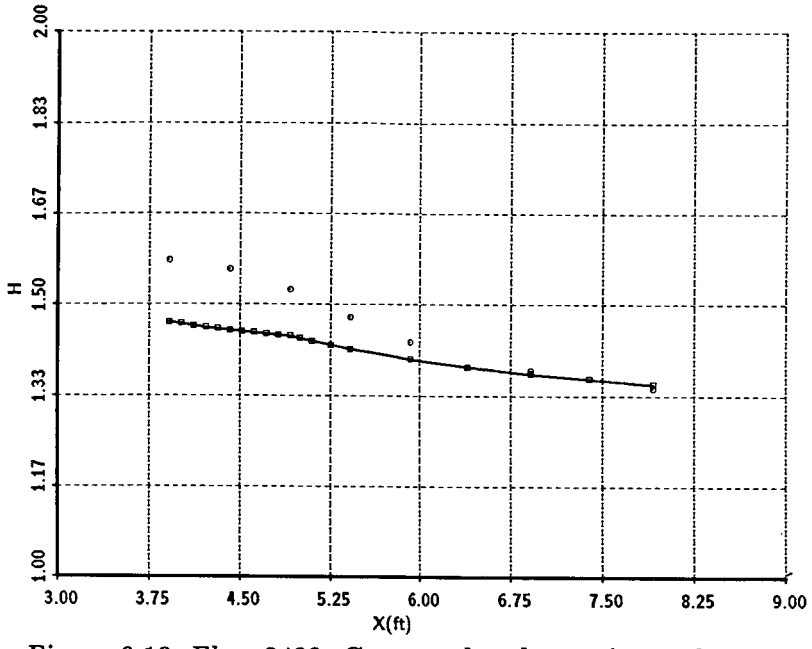

Figure 6.13: Flow 2400: Computed and experimental H

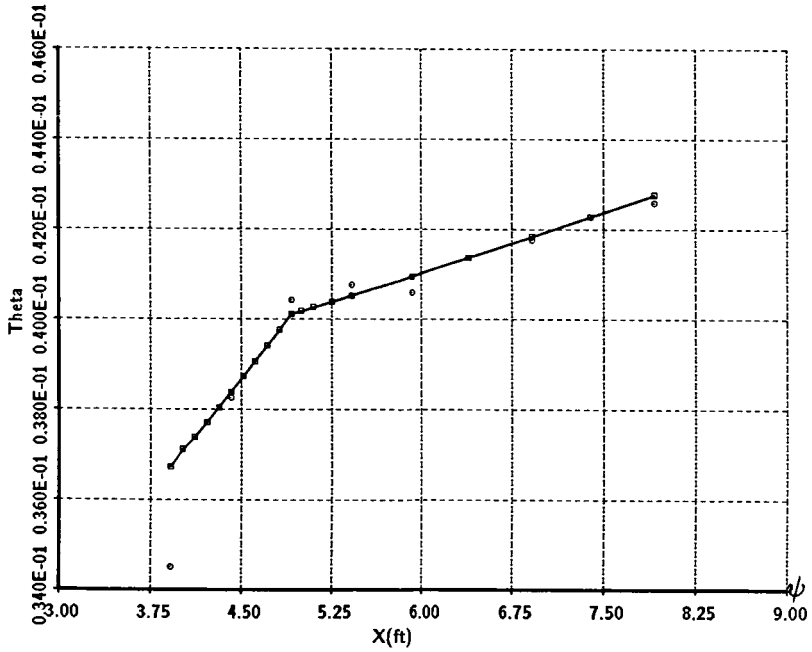

Figure 6.14: Flow 2400: Computed and experimental θ

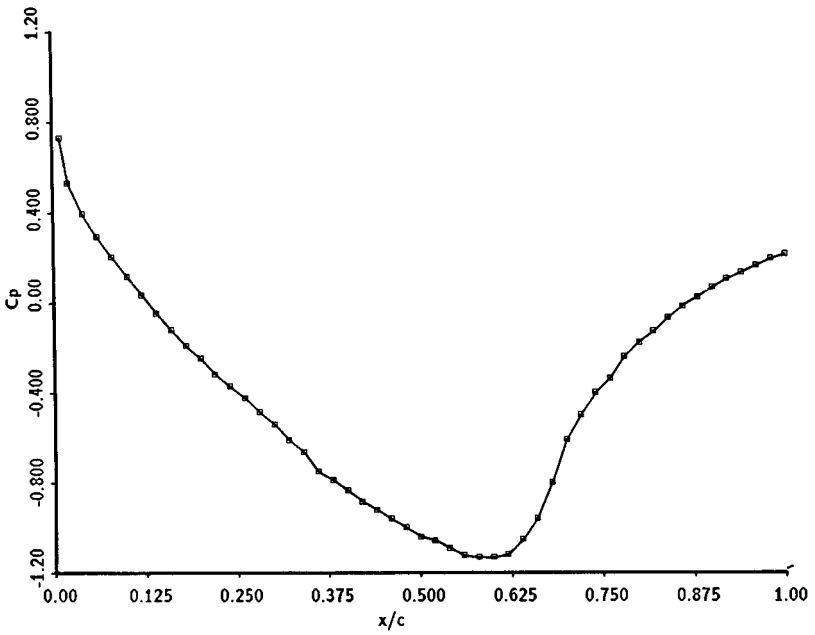

Figure 6.15: Circular arc airfoil: Pressure distribution

bulent boundary layer on a bicircular arc airfoil with 18% thickness ratio, at $M_\infty = 0.7425$, $Re_\infty = 4 \cdot 10^6$, and zero angle of attack. This flow case was previously calculated as a viscous/inviscid coupling problem by Wigton and Holt [Wigton 81]. They used a potential solver in the inviscid region, and Green's Lag entrainment scheme in the boundary layer. A plot of the pressure distribution calculated with their coupling scheme is shown in Fig. 6.15. The flow accelerates around the leading edge, goes through a weak shock at about 70% chord, decelerates, and separates just upstream of the trailing edge.

Specification of the edge velocity (direct mode) in the region of separated flow leads to an ill-posed set of equations. This problem can be circumvented by applying inverse boundary conditions to the problem – for example by specifying the wall shear or displacement thickness[5]. Also, to satisfy zone of dependency principles, the FLARE technique was implemented[6] We pose the problem as a mixed direct/inverse boundary condition problem, with

[5]This is discussed in detail in Appendix D.2

[6]...by setting $\int u d\psi_2 = \int u d\psi_4 = 0$ for $u_2 + u_4 \leq 0$. However, the energy equation was left unaltered since implementation of the FLARE technique there led to oscillations and instability in the total enthalpy.

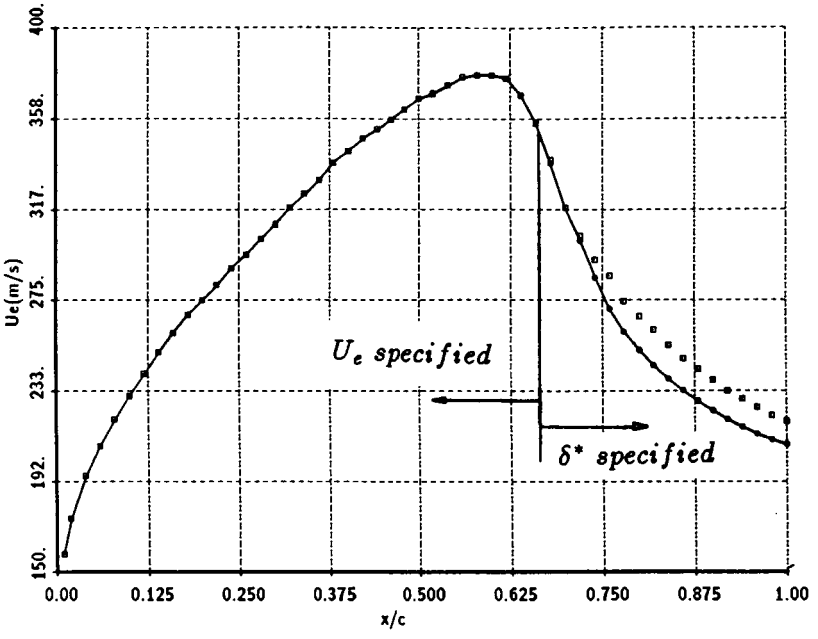

Figure 6.16: Circular arc airfoil: Edge Velocity

the edge velocity specified up to 68% chord, and the displacement thickness specified subsequently.

Some assumptions about the transition from laminar to turbulent flow must be made since [Wigton 81] does not discuss this issue. However, all figures of calculated quantities in [Wigton 81] begin at $x/c = 0.2$. Thus, we arbitrarily assumed the flow transitions to turbulence linearly between $x/c = 0.1$ and $x/c = 0.2$.

Figure 6.16 gives the edge velocity. Wigton's data is shown as unconnected symbols, while finite volume results are plotted as connected symbols. The edge velocity due to Wigton et al. was calculated from the reported pressure distribution (Fig. 6.15) by assuming constant stagnation pressure.

Figure 6.17 shows the displacement thickness as calculated (upstream of $x/c = 0.68$), and the results taken from [Wigton 81]. Downstream of $x/c = 0.68$ the two curves coincide since here displacement thickness was specified, and the agreement upstream of that point is excellent.

Figure 6.18 gives the finite volume skin friction results as well as the skin friction given in [Wigton 81] for $x/c > 0.2$. The agreement with Wigton's results is excellent up to about 70% chord, however the predictions of the

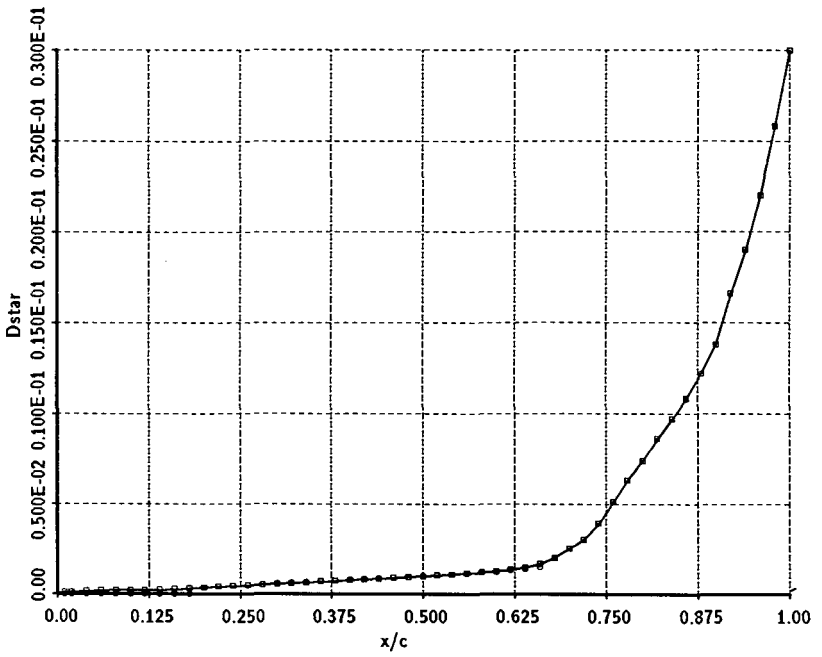

Figure 6.17: Circular arc airfoil: Displacement Thickness

separation point differ by about 5% chord. It is not clear which of the methods is in error, but we note that the Cebeci-Smith turbulence model is based on equilibrium boundary layer assumptions, and is not valid in or near separated zones.

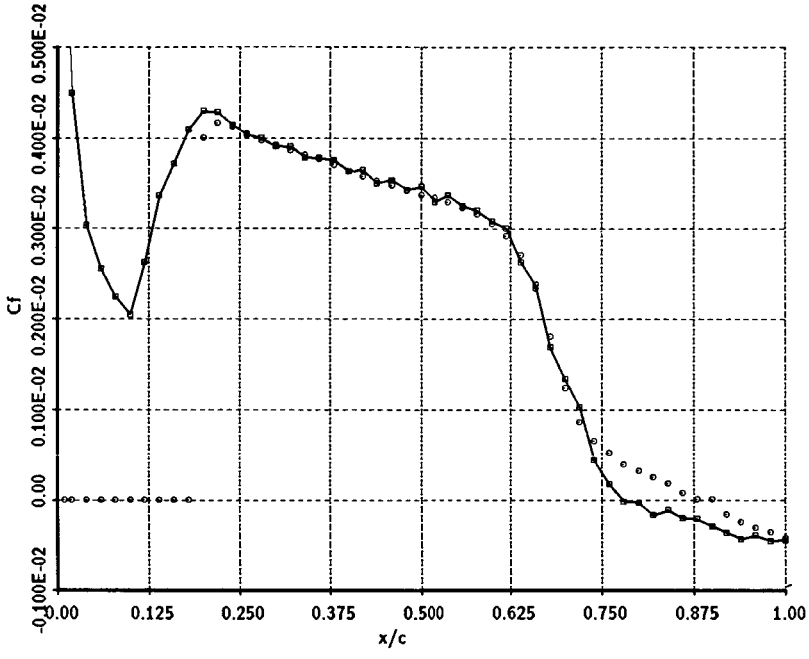

Figure 6.18: Circular arc airfoil: Skin Friction

Chapter 7

CONCLUSIONS

A finite volume method is applied to the compressible boundary layer equations. The novelty of our approach is the use of the integral form of the equations without transformation. Instead of incorporating similarity features into the governing equations via laborious transformations and scalings, we use similarity principles explicitly to generate the grid and calculate a starting solution. Instead of transforming the equations to remove the streamwise variation of flow variables in similar flow, we recognize the variation and correct for it explicitly when appropriate.

Important features of the method include:

- A simple untransformed stream function is used to simplify the governing equations.
- Similarity principles are used explicitly to generate a suitable computational grid, to calculate an initial solution, and to construct accurate flux formulae.
- The discrete finite volume equations are linearized and solved via Newton's method.
- Reynolds stress terms are calculated with the Cebeci-Smith algebraic two equation model.
- Diverse boundary conditions can be applied easily; the method does not distinguish between direct and inverse modes of calculation.

Results for similar flows and for compressible and turbulent test cases show excellent agreement with tabulated solutions and solutions obtained with a conventional method.

The explicit use of similarity is much simpler than the use of conventional transformations, but gives equivalent results. Our method retains the conceptual simplicity of the integral conservation equations without loosing the efficiency of conventional schemes. Extension to coupled inviscid-viscous calculations and to 3-dimensional flows (without the primitive variable formulation) should prove relatively straightforward. Thus, we recommend the method to potential users.

References

[Cebeci 74] Cebeci, T. and Smith, A.M.O., "Analysis of Turbulent Boundary Layers", Academic Press, New York, 1974.

[Coles 69] Coles, D. E. and Hirst E. A., editors, "Computation of Turbulent Boundary Layers", *Proc. of the 1968 AFOSR-IFP-Stanford Conference*, Volumes I & II, c. 1969.

[Drela 83] Drela, M., "A New Transformation and Integration Scheme for the Compressible Boundary Layer Equations, and Solution Behaviour at Separation", GTL Report 172, M. I. T., 1983.

[Keller 70] Keller, H.B., "Accurate Numerical Methods for Boundary Layer Flows: I. Two Dimensional Laminar Flows", *Proceedings of the Second International Conference on Numerical Methods in Fluid Dynamics*, Von Karman Institute for Fluid Dynamics, Sept. 15-19, 1970.

[Loyd 85] Loyd, B., "Finite Volume Solution of the Compressible Boundary Layer Equations", M. I. T. S.M. Thesis, June 1985.

[Schlichting 68] Schlichting, H., "Boundary-Layer Theory", Sixth ed. McGraw-Hill Book Co.,Inc., New York, c. 1968.

[Smith 78] Smith, G. D., "Numerical Solution of Partial Differential Equations: Finite Difference Methods", Clarendon Press, Oxford, 1978.

[Wigton 81] Wigton, L. B. and Holt M., "Viscous-Inviscid Interaction in Transonic Flow", AIAA-81-1003-CP, 1981.

Appendix A

EXACT FLUX CALCULATION

In similar flow, we know the power law behaviour of our variables along $\eta = const.$ All variables are of the form $k(x) = ax^{\phi}$, although ϕ may differ from variable to variable. We can apply this knowledge to calculate the exact fluxes through the streamwise grid lines.

Straightforward integration of $k(x)$ from x_i to x_{i+1} gives the exact flux:

$$\begin{aligned} k_e \,|_i^{i+1} &= \int_{x_i}^{x_{i+1}} ax^{\phi}\, dx \;=\; \frac{a}{\phi+1}\, x^{\phi+1} \;|_{x_i}^{x_{i+1}} \\ &= \frac{1}{\phi+1}(\, k_{i+1}x_{i+1} \;-\; k_i x_i\,), \end{aligned} \tag{A.1}$$

while our approximation to A.1

$$k_a \,|_i^{i+1} = .5 \cdot (k_{i+1} + k_i) \cdot (x_{i+1} - x_i), \tag{A.2}$$

is accurate to second order in Δx.

To examine the magnitude of the error define a flux correction factor α_c:

$$\alpha_c = \frac{\text{exact flux}}{\text{approx. flux}} = \frac{\frac{2}{\phi+1}(\, k_{i+1}x_{i+1} \;-\; k_i x_i\,)}{(k_{i+1} \;+\; k_i\,) \cdot (\, x_{i+1} \;-\; x_i\,)}, \tag{A.3}$$

For convenience, let $k_a \;= |_i^{i+1}$ and $k_e \;= |_i^{i+1}$. If $\alpha_c = 1$, the approximate flux, k_a, is equal to the exact flux, $k_(e)$. The larger the deviation of α_c from 1 the larger the error. Since (A.2) is a linear approximation, $\alpha_c = 1$ only if $k(x)$ is a constant or linear function of x ($\phi = 0$ or 1).

Formula A.3 is more instructive if we eliminate $x_{i+1}(= x_i + \Delta x_i)$, replace k_i by ax_i^{ϕ}, and manipulate the resulting expression to get

$$\alpha_c = \frac{2}{\phi+1}\frac{x_i}{\Delta x_i}\frac{(1+\Delta x_i/x_i)^{\phi+1}-1}{(1+\Delta x_i/x_i)^{\phi}+1} \tag{A.4}$$

Thus, for a given $\phi \neq 0$ or $1, \alpha_c$ is a function of $\Delta x_i/x_i$ only, and, for $\phi > 0$, is bounded by:

$$0 \leq \alpha_c \leq \frac{2}{\phi+1} \tag{A.5}$$

If $\Delta x_i/x_i$ is large (and $\phi \neq 0, 1$) $1-\alpha_c$ is large; as $\Delta x_i/x_i \rightarrow 0, \alpha_c \rightarrow 1$. We discuss specific applications of α_c, to fluxes calculated for incompressible stagnation and flat plate flow, below.

A.1 APPLICATION TO STAGNATION FLOW

For stagnation flow, simple averaging of the state vectors at i and $i+1$ to get the flux vectors is excellent, because all of the flow quantities vary linearly with x along constant η . Since $\phi = 1$, for both u and τ, our approximate flux calculations are exact: $\alpha_c = 1$, identically.

A.2 APPLICATION TO FLAT PLATE FLOW

In flat plate flow, u is constant along $\eta = const.$, and $\tau \sim x^{-1/2}$. Since U_e is constant, $\phi = \alpha_u = 0, \alpha_c = 1$ and our averaging will yield the exact fluxes u_1 and u_3. However, τ_1 and τ_3 will contain some error, since now $\phi = \alpha_t = -1/2$. Table A.2, below, gives α_c and the wall shear stress τ_w calculated for three values of $\Delta x/x$ and two different grid densities. τ_a and τ_e are the wall shear stresses calculated with k_a and k_e, respectively. For $\Delta x_i/x_i = 10$ and $\Delta x_i/x_i = 1$, the truncation error due to equation A.2 is large and causes significant error in the predicted value of τ_w. For $\Delta x_i/x_i \leq 0.1$, (A.2) is so accurate that correction is hardly necessary.

A cautionary note on the application of equation A.3 is in order. Clearly, potential benefits of its application occur only if

$$\Delta x_i/x_i >>\sim 0.1 \; . \tag{A.6}$$

However, application of (A.3) for situations where (A.6) holds guarantees only that the resulting solution is an accurate approximation to a similar

Table A.1: Wall Shear using approximate and exact flux calculations

$\Delta x_i/x_i$	α_c	# cells	τ_a	τ_e
10	0.7120	20	0.28122	0.33328
		40	0.28025	0.33237
1.0	0.9706	20	0.32834	0.33328
		40	0.32744	0.33237
0.1	0.9994	20	0.33319	0.33328
		40	0.33227	0.33237
			Exact: $\tau_w = 0.33206$	

flow at that station. If the flow is not similar to begin with, one is better off using the second order approximation without correction. Another potential application of (A.3) is near the leading edge in a flat plate type flow, since x_i may be quite small. This use is to be avoided, for it gives the mistaken impression that the solution has great physical merit. In fact, the flat plate boundary layer approximations are valid only for $Re_x >> 1$. Solutions of the complete Navier-Stokes equations near a leading edge indicate that profiles near $x = 0$ deviate significantly from boundary layer profiles. For these reasons, and for simplicity, use of (A.3) for nonsimilar calculations is of dubious benefit and is not recommended.

Appendix B

SUTHERLAND'S LAW

Sutherland models the dependence of viscosity on temperature with

$$\frac{\mu}{\mu_0} = \left(\frac{T}{T_0}\right)^{3/2} \frac{T_0 + T_1}{T + T_1} \,. \tag{B.1}$$

μ_0 is the viscosity at a reference temperature T_0. T_1 is a constant: for air $T_1 \approx 110\ K$.

Equation B.1 may be written in terms of the enthalpy $h = C_p \cdot T$,

$$\frac{\mu}{\mu_0} = \left(\frac{h}{h_0}\right)^{3/2} \frac{h_0 + h_1}{h + h_1} \,, \tag{B.2}$$

by assuming a constant specific heat.

Appendix C

CEBECI-SMITH TURBULENCE MODEL

We use the Cebeci-Smith two equation model to give the eddy viscosity, μ_t. We outline the relevant equations here, and recommend the thorough discussion of the model in [Cebeci 74].

The model is based on Prandtl's mixing length theory or, equivalently, on the Boussinesq eddy-viscosity concept. The Boussinesq formulation models the Reynolds stress in the form

$$\tau_t = -\rho\overline{u'v'} = \rho\epsilon_m \frac{\partial u}{\partial y}. \tag{C.1}$$

The Cebeci-Smith model describes the variation of the eddy viscosity in the inner and outer regions of turbulent boundary layers by the formulae:

$$\begin{aligned} \epsilon_{m_i} &= L^2 \left|\frac{\partial u}{\partial y}\right| \gamma_{tr} && 0 < y < y_c \\ \epsilon_{m_o} &= \alpha U_e \delta_k^* \gamma_{tr} && y_c < y < y_e \ , \end{aligned} \tag{C.2}$$

where L is a mixing length, δ_k^* is the kinematic displacement thickness, γ_{tr} is an intermittency factor, and α is a function of the Reynolds number. y_c is the normal location where $\epsilon_{m_i} = \epsilon_{m_o}$.

In the inner layer, the mixing length L is proportional to the distance y from the wall, $L = \kappa y$. The formula for the inner region is accurate in the sublayer and buffer layer if the Van Driest modification for the mixing length is used:

$$\kappa = \kappa_o(1 - e^{-y/A}), \tag{C.3}$$

where the Karman constant κ_o is generally taken to be equal to 0.4, and A is the Van Driest damping parameter as modified by Cebeci.

A takes pressure gradients and/or mass transfer into account:

$$A = A^+ \frac{\nu}{N} \left[\frac{\tau_w}{\rho_w}\right]^{-1/2} \left[\frac{\rho}{\rho_w}\right]^{1/2} \tag{C.4}$$

where $A^+ = 26$, and

$$N = \left[1 - 11.8 \left[\frac{\mu_w}{\mu_e}\right] \left[\frac{\rho_e}{\rho_w}\right]^2 P^+\right]^{1/2} . \tag{C.5}$$

P^+ is a pressure gradient

$$P^+ = \left[\frac{\nu_e U_e}{U_\tau^3}\right] \frac{dU_e}{dx}, \tag{C.6}$$

and U_τ is the friction velocity

$$U_\tau = \left[\frac{\tau_w}{\rho_w}\right]^{1/2} . \tag{C.7}$$

The above formulae used with constant α give accurate results for large Reynolds numbers. For small Reynolds numbers agreement with experimental results is improved by introducing a variable α. For $R_{\theta_k} = \frac{U_e \theta_k}{\nu} < 5000$, $\alpha = f(R_{\theta_k})$ as follows:

$$\alpha = \alpha_o \frac{1 + \pi_o}{1 + \pi} \tag{C.8}$$

$$\pi_o = 0.55 \qquad\qquad \alpha_o = 0.0168 \tag{C.9}$$

where

$$\pi = \pi_o \left[1 - exp(-0.243 z_1^{1/2} - 0.298 z_1)\right], \tag{C.10}$$

and

$$z_1 = \frac{R_{\theta_k}}{425} - 1 . \tag{C.11}$$

The intermittency factor γ may be user prescribed or experimentally defined.

C.1 NON-DIMENSIONALIZATION

We non-dimensionalize equations C.2 to C.11, above, to be consistent with the non-dimensionalization introduced in Section 2.2. The form of the non-dimensioned equations turns out to be identical to the form of the dimensioned equations (a consequence of the dimensional consistency of the model and the "natural" non-dimensionalization). We demonstrate this below.

It is convenient to start with the inner model. In non-dimensioned quantities (simply plugging in relations 2.8), the shear velocity is

$$U_\tau = \left[\rho_\infty U_\infty^2\right]^{1/2} \left[\frac{1}{\rho_\infty}\right]^{1/2} \left[\frac{\tau_w'}{\rho_w'}\right]^{1/2}. \tag{C.12}$$

As before, primes (') denote non-dimensioned quantities. Equation C.12 suggests a non-dimensioned friction velocity

$$U_\tau' = \frac{U_\tau}{U_\infty} = \left[\frac{\tau_w'}{\rho_w'}\right]^{1/2}. \tag{C.13}$$

Now P^+ becomes

$$P^+ = [U_\infty L_\infty]\, \nu_e' [U_\infty]\, U_e' \frac{1}{[U_\infty U_\tau']^3} \left[\frac{U_\infty}{L_\infty}\right] \frac{dU_e'}{dx'} \tag{C.14}$$

$$P^{+'} = P^+ = \left[\frac{\nu_e' U_e'}{U_\tau'^3}\right] \frac{dU_e'}{dx'}. \tag{C.15}$$

N is also dimensionless:

$$N = N' = \left[1 - 11.8 \left[\frac{\mu_w'}{\mu_e'}\right] \left[\frac{\rho_e'}{\rho_w'}\right]^2 P^{+'}\right]^{1/2}, \tag{C.16}$$

whereas A becomes

$$A = A^+ [U_\infty L_\infty] \frac{\nu'}{N'} \left[\frac{1}{U_\infty U_\tau'}\right] \left[\frac{\rho'}{\rho_w'}\right]^{1/2} \tag{C.17}$$

$$A' = \frac{A}{L_\infty} = A^+ \frac{\nu'}{N'} \left[\frac{1}{U_\tau'}\right] \left[\frac{\rho'}{\rho_w'}\right]^{1/2}, \tag{C.18}$$

consistent with

$$L' = \frac{L}{L_\infty} = \kappa' y' \tag{C.19}$$

and

$$\kappa' = \kappa = \kappa_o(1 - e^{-y'/A'}) \,. \tag{C.20}$$

The coefficient α in equation C.8 is dimensionless; thus, we consider equations C.2. These become

$$\epsilon_{m_i} = \left[L_\infty^2\right] \left[\kappa y'\right]^2 \left[\frac{U_\infty}{L_\infty}\right] \left[\frac{\partial u'}{\partial y'}\right] \gamma_{tr} \tag{C.21}$$

and

$$\epsilon_{m_o} = \left[U_\infty L_\infty\right] \alpha U_e' \delta_k'^* \gamma_{tr}, \tag{C.22}$$

so that

$$\epsilon' = \frac{\epsilon}{U_\infty L_\infty} = \begin{cases} L'^2 \left|\partial u'/\partial y'\right| \gamma_{tr} & 0 < y < y_c \\ \alpha U_e' \delta_k'^* \gamma_{tr} & y_c < y < y_e \end{cases} \tag{C.23}$$

As promised, equations C.23 are identical in form to equations C.2.

Appendix D

GLOBAL UNKNOWNS

This appendix describes the process of including (and solving for) global unknowns in the system of equations. Recall that the solution vector is of the form

$$\begin{aligned} \Delta u_j &= a_{j,1} - b_{j,1}\Delta\theta_k - c_{j,1}\Delta U_e \\ \Delta\psi_j &= a_{j,2} - b_{j,2}\Delta\theta_k - c_{j,2}\Delta U_e \\ \Delta\tau_j &= a_{j,3} - b_{j,3}\Delta\theta_k - c_{j,3}\Delta U_e \\ \Delta H_j &= a_{j,4} - b_{j,4}\Delta\theta_k - c_{j,4}\Delta U_e \\ \Delta q_j &= a_{j,5} - b_{j,5}\Delta\theta_k - c_{j,5}\Delta U_e \end{aligned} \tag{D.1}$$

The influence coefficient vectors a, b, and c are known. $\Delta\theta_k$ and ΔU_e are global unknowns that must be determined by specifying two auxillary relations in the form:

$$\begin{aligned} A_1\Delta\theta_k + B_1\Delta U_e &= R_1 \\ A_2\Delta\theta_k + B_2\Delta U_e &= R_2 \end{aligned} \tag{D.2}$$

One of these relations must result from specifying a fifth boundary condition, the other can be derived from the definition of y_e. The derivation of equation D.2 for both cases is discussed below.

Consider the calculation of the grid edge y_e as part of the solution at each streamwise station. We wish to impose a condition that ensures that $y_e(x)$ is always greater than the boundary layer thickness. In most boundary layer flows, the kinematic (incompressible) momentum thickness θ_k is a good measure of the boundary layer thickness [Drela 83]. Thus we define

$$y_e = \eta_e\theta_k\,, \tag{D.3}$$

where η_e is a constant[1] chosen such that $y_e > \delta$.

[1] Generally $\eta_e = 15$, 18 for laminar and turbulent flows, respectively, is adequate.

θ_k is defined as:

$$\theta_k = \int_0^{y_e} \frac{u}{U_e}\left[1 - \frac{u}{U_e}\right] dy$$

or, using equation D.3,

$$1 = \int_0^{\eta_e} \frac{u}{U_e}\left[1 - \frac{u}{U_e}\right] d\eta \tag{D.4}$$

Equation D.4 implies equation D.3. Thus, we include it as an auxillary relation in the Newton system of equations.

Newton linearization of eqn. D.4 proceeds as before. We need

$$Res_{\theta_k} + \frac{\partial Res_{\theta_k}}{\partial u_{j+1}}\Delta u_{j+1} + \frac{\partial Res_{\theta_k}}{\partial u_j}\Delta u_j + ... = 0\,. \tag{D.5}$$

Discretizing D.4 gives:

$$Res_{\theta_k} = \sum_{j=1}^{J-1} \frac{(u_{j+1}+u_j)}{2U_e}\left[1 - \frac{u_{j+1}+u_j}{2U_e}\right](\eta_{j+1} - \eta_j) - 1 \tag{D.6}$$

and

$$\frac{\partial Res_{\theta_k}}{\partial u_j} = \frac{\partial Res_{\theta_k}}{\partial u_{j+1}} = \left[\frac{1}{2U_e} - \frac{u_{j+1}+u_j}{2U_e^2}\Delta\eta_j\right] \tag{D.7}$$

Inserting D.6 - D.7 into D.5 gives

$$\sum_{j=1}^{J-1}(\Delta u_{j+1}+\Delta u_j)(1-\frac{u_{j+1}+u_j}{U_e})\frac{\Delta\eta_j}{2} = \sum_{j=1}^{J-1}\left[\frac{u_{j+1}+u_j}{2}\right]\left[1 - \frac{u_{j+1}+u_j}{2U_e}\right]\Delta\eta_j - U_e$$

which, upon transposing and defining $u_{ave} = .5(u_{j+1} + u_j)$, simplifies to

$$\sum_{j=1}^{J-1}\left[(\Delta u_{j+1} + \Delta u_j)(1/2 - u_{ave}/U_e) - u_{ave}(1 - u_{ave}/U_e)\right]\Delta\eta_j = -U_e \tag{D.8}$$

Equation D.8 is the first of the two additional relations needed to close the system of equations. However, the δu_j's in D.8 are unknown and must be related to the global unknowns. We eliminate Δu_{j+1} and Δu_j by using relations D.1 from the factorized system of equations:

$$\begin{aligned} \Delta u_j &= a_{j,1} - b_{j,1}\Delta\theta_k - c_{j,1}\Delta U_e \\ \Delta u_{j+1} &= a_{j+1,1} - b_{j+1,1}\Delta\theta_k - c_{j+1,1}\Delta U_e \end{aligned} \tag{D.9}$$

Plugging these into Eqn. D.8 and moving known quantities to the right hand side gives the required form D.2:

$$\sum_{j=1}^{J-1} \{[(b_{j,1} + b_{j+1,1})\Delta\theta_k + (c_{j,1} + c_{j+1,1})\Delta U_e]\,(1/2 - u_{ave}/U_e)\Delta\eta_j\} =$$

$$U_e + \sum_{j=1}^{J-1} \{[(a_{j,1} + a_{j+1,1})(1/2 - u_{ave}/U_e) - u_{ave}(1 - u_{ave}/U_e)]\,\Delta\eta_j\}$$

or

$$\begin{aligned} A_1 &= \sum_{j=1}^{J-1} (b_{j,1} + b_{j+1,1})(1/2 - u_{ave}/U_e)\Delta\eta_j \\ B_1 &= \sum_{j=1}^{J-1} (c_{j,1} + c_{j+1,1})(1/2 - u_{ave}/U_e)\Delta\eta_j \end{aligned} \tag{D.10}$$

and

$$R_1 = U_e + \sum_{j=1}^{J-1} [(a_{j,1} + a_{j+1,1})(1/2 - u_{ave}/U_e) - u_{ave}(1 - u_{ave}/U_e)]\,\Delta\eta_j \tag{D.11}$$

The second equation in D.2 is obtained by imposing any one of a number of possible boundary conditions. Here we discuss specifying edge velocity, wall shear, or displacement thickness; however, other boundary conditions can be easily implemented.

1. Specified edge velocity (direct mode):

$$U_e - \Delta U_e \equiv U_{spec}$$

where U_{spec} is the specified edge velocity. Thus

$$\begin{aligned} A_2 &= 0 \\ B_2 &= -1 \\ R_2 &= U_{spec} - U_e \end{aligned} \tag{D.12}$$

2. Specified wall shear (inverse mode):

$$\tau_1 - \Delta\tau_1 \equiv \tau_{spec}\ .$$

Using equation D.1

$$\Delta\tau_1 = a_{j=1,3} - b_{j=1,3}\Delta\theta_k - c_{j=1,3}\Delta U_e\ ,$$

gives

$$\tau_{spec} - \tau_1 = -a_{j=1,3} + b_{j=1,3}\Delta\theta_k + c_{j=1,3}\Delta U_e \,, \tag{D.13}$$

so that

$$\begin{aligned} A_2 &= b_{j=1,3} \\ B_2 &= c_{j=1,3} \\ R_2 &= \tau_{spec} - \tau_1 + a_{j=1,3} \end{aligned} \tag{D.14}$$

3. Specified displacement thickness (inverse mode):

$$\delta^* - \Delta\delta^* \equiv \delta_{spec}$$

Displacement thickness is defined as

$$\begin{aligned} \delta^* &= \int_0^{y_e} \left[1 - \frac{\rho u}{\rho_e U_e}\right] dy \\ &= \int_0^{y_e} \left[1 - \frac{1}{\rho_e U_e}\frac{\partial \psi}{\partial y}\right] dy \\ &= y_e - \frac{1}{\rho_e U_e}(\psi_e - \psi_w) \end{aligned}$$

Thus,

$$-\Delta\delta^* = \delta_{spec} - y_J + \frac{1}{\rho_J U_J}\psi_J \quad (\psi_w = 0) \,. \tag{D.15}$$

The left hand side of [D.15] is

$$\Delta\delta^* = \frac{\partial \delta^*}{\partial \theta_k}\Delta\theta_k + \frac{\partial \delta^*}{\partial U_J}\Delta Ue + \frac{\partial \delta^*}{\partial \psi_J}\Delta\psi_J \,, \tag{D.16}$$

via the chain rule, with

$$\begin{aligned} \partial\delta^*/\partial\theta_k &= \eta_J \\ \partial\delta^*/\partial U_J &= \frac{\psi_J}{\rho_J U_J}\left[\frac{1}{U_J} + \frac{1}{\rho_J}\frac{\partial \rho_J}{\partial U_J}\right] \\ \partial\delta^*/\partial\psi_J &= -1/(\rho_J U_J) \end{aligned} \tag{D.17}$$

Inserting these relations into [D.15] gives

$$-\eta_J\Delta\theta_k - \frac{\psi_J}{\rho_J U_J^2}\Delta U_J + \frac{1}{\rho_J U_J}\Delta\psi_J = \delta^*_{spec} - y_J + \frac{1}{\rho_J U_J}\psi_J \,.$$

Eliminating $\Delta\psi_J$ via

$$\Delta\psi_J = a_{J,2} - b_{J,2}\Delta\theta_k - c_{J,2}\Delta U_J$$

allows us to write this in the usual form (D.2) where

$$\begin{aligned} A_2 &= -\eta_J - b_{J,2}/(\rho_J U_J) \\ B_2 &= -\left(\psi_J\left[\tfrac{1}{U_J} + \tfrac{1}{\rho_J}\tfrac{\partial\rho_J}{\partial U_J}\right] + c_{J,2}\right)\tfrac{1}{\rho_J U_J} \\ R_2 &= \delta^*_{spec} - y_J + (\psi_J - a_{J,2})/(\rho_J U_J) \end{aligned} \qquad \text{(D.18)}$$

Appendix E

NEWTON SYSTEM

This appendix lists vectors and block matrices defined in the Newton system for incompressible laminar flow. In general, $\Delta's$ indicate the difference of a quantity taken in the counter-clockwise sense. The exceptions to this rule is $\Delta\eta$ which is defined as $\eta_{j+1} - \eta_j$ and Δx which is defined as $x_{i+1} - x_i$. Quantities with numerical subscripts, say H_2, are defined as the average of H at the adjacent node points. Demonstrative examples of these conventions are:

$$\begin{array}{llll} \Delta u_2 & = u_{i+1,j+1} - u_{i+1,j} & u_2 & = .5(u_{i+1,j+1} + u_{i+1,j}) \\ \Delta y_2 & = \theta_{i+1}\Delta\eta_j & u_3 & = .5(u_{i,j+1} + u_{i+1,j+1}) \end{array} \qquad \text{(E.1)}$$

The linear equations corresponding to each residual equation in the Newton system 5.4 can be written in block tridiagonal form. For an incompressible model, this is matrix equation E.2 below. Note that the residuals corresponding to a given cell are shifted by two equations with respect to the block structure, due to imposition of the boundary conditions at the wall.

$$
\begin{bmatrix}
1 & 0 & 0 & 0 & 0 & 0 & & & & & & \\
0 & 1 & 0 & 0 & 0 & 0 & & 0 & & & 0 & \\
\frac{\partial R_{r_1}}{\partial u_1} & \frac{\partial R_{r_1}}{\partial \psi_1} & \frac{\partial R_{r_1}}{\partial \tau_1} & \frac{\partial R_{r_1}}{\partial u_2} & \frac{\partial R_{r_1}}{\partial \psi_2} & \frac{\partial R_{r_1}}{\partial \tau_2} & & & & & & \\
\frac{\partial R_{u_1}}{\partial u_1} & \frac{\partial R_{u_1}}{\partial \psi_1} & \frac{\partial R_{u_1}}{\partial \tau_1} & \frac{\partial R_{u_1}}{\partial u_2} & \frac{\partial R_{u_1}}{\partial \psi_2} & \frac{\partial R_{u_1}}{\partial \tau_2} & 0 & 0 & 0 & & & \\
\frac{\partial R_{\psi_1}}{\partial u_1} & \frac{\partial R_{\psi_1}}{\partial \psi_1} & \frac{\partial R_{\psi_1}}{\partial \tau_1} & \frac{\partial R_{\psi_1}}{\partial u_2} & \frac{\partial R_{\psi_1}}{\partial \psi_2} & \frac{\partial R_{\psi_1}}{\partial \tau_2} & 0 & 0 & 0 & & 0 & \\
0 & 0 & 0 & \frac{\partial R_{r_2}}{\partial u_2} & \frac{\partial R_{r_2}}{\partial \psi_2} & \frac{\partial R_{r_2}}{\partial \tau_2} & \frac{\partial R_{r_2}}{\partial u_3} & \frac{\partial R_{r_2}}{\partial \psi_3} & \frac{\partial R_{r_2}}{\partial \tau_3} & & & \\
 & & & & \cdots & & & \cdots & & & \cdots & \\
 & 0 & & & \cdots & & & \cdots & & & \cdots & \\
 & & & & \cdots & & & \cdots & & & \cdots & \\
 & & & & & & \frac{\partial R_{u_J}}{\partial u_J} & \frac{\partial R_{u_J}}{\partial \psi_J} & \frac{\partial R_{u_J}}{\partial \tau_J} & \frac{\partial R_{u_J}}{\partial u_{J+1}} & \frac{\partial R_{u_J}}{\partial \psi_{J+1}} & \frac{\partial R_{u_J}}{\partial \tau_{J+1}} \\
 & 0 & & & 0 & & \frac{\partial R_{\psi_J}}{\partial u_J} & \frac{\partial R_{\psi_J}}{\partial \psi_J} & \frac{\partial R_{\psi_J}}{\partial \tau_J} & \frac{\partial R_{\psi_J}}{\partial u_{J+1}} & \frac{\partial R_{\psi_J}}{\partial \psi_{J+1}} & \frac{\partial R_{\psi_J}}{\partial \tau_{J+1}} \\
 & & & & & & 0 & 0 & 0 & 1 & 0 & 0
\end{bmatrix}
\begin{bmatrix}
\delta u_1 \\ \delta \psi_1 \\ \delta \tau_1 \\ \delta u_2 \\ \delta \psi_2 \\ \delta \tau_2 \\ .. \\ .. \\ .. \\ \delta u_{J+1} \\ \delta \psi_{J+1} \\ \delta \tau_{J+1}
\end{bmatrix} =
$$

$$
= \begin{bmatrix} 0 \\ 0 \\ R_{r_1} \\ R_{u_1} \\ R_{\psi_1} \\ R_{r_2} \\ .. \\ .. \\ .. \\ R_{u_J} \\ R_{\psi_J} \\ 0 \end{bmatrix} - \Delta\theta_k \begin{bmatrix} 0 \\ 0 \\ \frac{\partial R_{r_1}}{\partial \theta_k} \\ \frac{\partial R_{u_1}}{\partial \theta_k} \\ \frac{\partial R_{\psi_1}}{\partial \theta_k} \\ \frac{\partial R_{r_2}}{\partial \theta_k} \\ .. \\ .. \\ .. \\ \frac{\partial R_{u_J}}{\partial \theta_k} \\ \frac{\partial R_{\psi_J}}{\partial \theta_k} \\ 0 \end{bmatrix} - \Delta U_e \begin{bmatrix} 0 \\ 0 \\ \frac{\partial R_{r_1}}{\partial U_e} \\ \frac{\partial R_{u_1}}{\partial U_e} \\ \frac{\partial R_{\psi_1}}{\partial U_e} \\ \frac{\partial R_{r_2}}{\partial U_e} \\ .. \\ .. \\ .. \\ \frac{\partial R_{u_J}}{\partial U_e} \\ \frac{\partial R_{\psi_J}}{\partial U_e} \\ 0 \end{bmatrix} \qquad \text{(E.2)}
$$

J computational cells result in $J+1$ unknown changes (δ 's), and J conservation equations. Boundary conditions are implemented in the first, second and final equations of the block matrix. The conservation equations run from equations 3 through $3*J-1$ and, due to the boundary conditions, are shifted with respect to the block structure.

Below are the matrices and vectors that make up the Newton system. The vector of residuals is:

$$R_1 = \begin{bmatrix} 0 \\ 0 \\ \tau_2 \Delta y_2 - \mu \Delta u_2 \end{bmatrix} \tag{E.3}$$

$$R_j = \begin{bmatrix} (u_1 \Delta\psi_1 + u_3 \Delta\psi_3 + P_1(\Delta y_1 + \Delta y_3) + (\tau_1 - \tau_3)\Delta x) \\ \quad +(u_2 \Delta\psi_2 + u_4 \Delta\psi_4 + (P_2 \Delta y_2 + P_4 \Delta y_4)) \\ \Delta\psi_2 - u_2 \Delta y_2 \\ \tau_2 \Delta y_2 - \mu \Delta u_2 \end{bmatrix} \tag{E.4}$$

$$R_J = \begin{bmatrix} (u_1 \Delta\psi_1 + u_3 \Delta\psi_3 + P_1(\Delta y_1 + \Delta y_3) + (\tau_1 - \tau_3)\Delta x) \\ \quad +(u_2 \Delta\psi_2 + u_4 \Delta\psi_4 + (P_2 \Delta y_2 + P_4 \Delta y_4)) \\ \Delta\psi_2 - u_2 \Delta y_2 \\ 0 \end{bmatrix} \tag{E.5}$$

The Jacobian block matrices A, B, and C are:

$$A_j = \begin{bmatrix} 1 & 0 & 0 \\ 0 & 1 & 0 \\ \mu & 0 & .5\Delta y_2 \end{bmatrix} \tag{E.6}$$

$$A_j = \begin{bmatrix} .5(\Delta\psi_3 + \Delta\psi_2) & u_2 - u_3 & -\Delta x \\ -.5\Delta y_2 & 1. & 0 \\ \mu & 0 & .5\Delta y_2 \end{bmatrix} \tag{E.7}$$

$$A_J = \begin{bmatrix} .5(\Delta\psi_3 + \Delta\psi_2) & u_2 - u_3 & -\Delta x \\ -.5\Delta y_2 & 1. & 0 \\ 1 & 0 & 0 \end{bmatrix} \tag{E.8}$$

$$B_j = \begin{bmatrix} .5(\Delta\psi_1 + \Delta\psi_2) & u_1 - u_2 & \Delta x \\ -.5\Delta y_2 & -1. & 0 \\ 0 & 0 & 0 \end{bmatrix} \tag{E.9}$$

$$C_j = \begin{bmatrix} 0 & 0 & 0 \\ 0 & 0 & 0 \\ -\mu & 0 & .5\Delta y_2 \end{bmatrix} \tag{E.10}$$

Laminar flow has been assumed for simplicitiy. If in fact a turbulence model is implemented it is very important to linearize this as well.

The vectors G and H are:

$$G_1 = \begin{bmatrix} 0 \\ 0 \\ \tau_2 \Delta\eta_1 \end{bmatrix} \quad G_j = \begin{bmatrix} (P_2 - P_1)\Delta\eta_j \\ -u_2\Delta\eta_j \\ \tau_2\Delta\eta_j \end{bmatrix} \quad G_J = \begin{bmatrix} (P_2 - P_1)\Delta\eta_j \\ -u_2\Delta\eta_j \\ 0 \end{bmatrix} \tag{E.11}$$

$$H_1 = \begin{bmatrix} 0 \\ 0 \\ 0 \end{bmatrix} \quad H_j = \begin{bmatrix} -.5u_{i+1,J}((\Delta y_1 + \Delta y_3) + 2\Delta y_2) \\ 0 \\ 0 \end{bmatrix} \tag{E.12}$$

$$H_{J-1} = \begin{bmatrix} -.5u_{i+1,J}((\Delta y_1 + \Delta y_3) + 2\Delta y_2) \\ 0 \\ C_{J,3,1} \end{bmatrix} \tag{E.13}$$

$$H_J = \begin{bmatrix} -.5u_{i+1,J}((\Delta y_1 + \Delta y_3) + 2\Delta y_2) + A_{J,1,1} \\ A_{J,2,1} \\ 0 \end{bmatrix} \tag{E.14}$$

E.1 INITIAL CONDITIONS

The above vectors and block matrices must be modified at the initial station. In the following matrices, it is assumed that a solution is sought at face 4 (East) and variables are extrapolated from face 4 to face 2 (West) to obtain ordinary *difference* equations[1]. Thus, the definitions of the stream function, shear stress, and enthalpy flux and their corresponding entries,since they contain no terms at face 4, are identical to the marching case. Only the entries corresponding to the momentum and energy equations are slightly different; and, for this incompressible case, we need give only the first row/entry in each of the matrices/vectors.

Some new definitions are (to implement similarity principles):

$$x_u = (x_i/x_{i+1})^{\alpha_u}, \quad x_t = (x_i/x_{i+1})^{\alpha_t}$$

[1]Alternatively, the solution could be sought at face 2 and variables extrapolated from face 2 to face 4.

$$x_s = (x_i/x_{i+1})^{\alpha_s}, \quad x_y = (x_i/x_{i+1})^{\alpha_y}$$

$$x_{u13} = 1 + x_u, \quad x_{t13} = 1 + x_t$$

$$x_{s13} = 1 - x_s, \quad x_{y13} = 1 - x_y \ .$$

With these definitions, the following identities are true in similar flow:

$$\Delta\psi_1 = -\psi_{i,j}x_{s13}, \quad \Delta\psi_3 = \psi_{i,j+1}x_{s13}$$

$$\Delta\psi_2 = -\Delta\psi_4 x_s, \quad \text{etc. for } \Delta y$$

and

$$u_1 = .5u_{i,j}x_{u13}, \quad u_3 = .5u_{i,j+1}x_{u13}$$

$$u_2 = .5u_4 x_u, \quad \text{etc. for } \tau,\ H,\ q\ ,\psi\ .$$

$$R_{j,1} = \left[\begin{array}{c} (u_1\Delta\psi_1 + u_3\Delta\psi_3 + P_1(\Delta y_1 + \Delta y_3) + (\tau_1 - \tau_3)\Delta x) \\ +(u_2\Delta\psi_2 + u_4\Delta\psi_4 + (P_2\Delta y_2 + P_4\Delta y_4)) \end{array} \right] \tag{E.15}$$

$$B_{j,row1} = \left[.5(x_{u13}\Delta\psi_1 + \Delta\psi_2 x_u + \Delta\psi_4) \quad -u_1x_{s13} - u_2x_s + u_4 \quad .5x_{t13}\Delta x \right] \tag{E.16}$$

$$A_{j,row1} = \left[.5(x_{u13}\Delta\psi_3 + \Delta\psi_2 x_u + \Delta\psi_4) \quad u_3x_{s13} + u_2x_s - u_4 \quad .5x_{t13}\Delta x \right] \tag{E.17}$$

$$G_{j,1} = \left[\ (P_1(\Delta y_1 + \Delta y_3) + P_2\Delta y_2 + P_4\Delta y_4)/\theta_i \ \right] \tag{E.18}$$

$$H_{j,1} = \left[\begin{array}{c} -.5u_{i,J}((1 + x_u^2) * (\Delta y_1 + \Delta y_3) \\ +2(x_u^2\Delta y_2 + \Delta y_4)) \end{array} \right] \tag{E.19}$$

Clearly, changes in the discrete equations to allow calculation of an initial solution are minor and can easily be included as a special case of the marching solution. The omitted matrices and vectors (at $j = 1$, $j = J - 1$, and $j = J$) can be constructed by simple analogy with the marching solution setup above.

Appendix F

PROGRAM LISTING

A program listing of the *FORTRAN* computer code is available upon request.

Standard Bibliographic Page

1. Report No.	2. Government Accession No.	3. Recipient's Catalog No.
NASA CR-4013		

4. Title and Subtitle	5. Report Date
Finite Volume Solution of the Compressible Boundary-Layer Equations	October 1986
	6. Performing Organization Code
7. Author(s)	8. Performing Organization Report No.
Bernard Loyd and Earll M. Murman	CFDL TR-86-1
9. Performing Organization Name and Address	10. Work Unit No.
Massachusetts Institute of Technology Department of Aeronautics and Astronautics Cambridge, MA 02139	11. Contract or Grant No. NAG1-507
12. Sponsoring Agency Name and Address	13. Type of Report and Period Covered
National Aeronautics and Space Administration Washington, DC 20546	Contractor Report
	14. Sponsoring Agency Code 505-90-11-01

15. Supplementary Notes

Langley Technical Monitor: James C. Townsend

16. Abstract

A box-type finite volume discretization is applied to the integral form of the compressible boundary layer equations. Boundary layer scaling is introduced through the grid construction: streamwise grid lines follow $\eta = y/h = const.$, where y is the normal coordinate and $h(x)$ is a scale factor proportional to the boundary layer thickness. With this grid, similarity can be applied explicitly to calculate initial conditions. The finite volume method preserves the physical transparency of the integral eqautions in the discrete approximation. The resulting scheme is accurate, efficient, and conceptually simple. Computations for similar and non-similar flows show excellent agreement with tabulated results, solutions computed with Keller's Box scheme, and experimental data.

17. Key Words (Suggested by Authors(s))	18. Distribution Statement
Boundary layers Compressible flow Finite volume method Box scheme	Unclassified - Unlimited Subject Category 64

19. Security Classif.(of this report)	20. Security Classif.(of this page)	21. No. of Pages	22. Price
Unclassified	Unclassified	80	A05

For sale by the National Technical Information Service, Springfield, Virginia 22161

NASA-Langley, 1986